JGR Atmospheres

RESEARCH ARTICLE
10.1029/2020JD034164

New Observation Operators for Cloud Liquid/Ice Water Path From ABI and Their Impact on Assimilation and Hurricane Forecasts

Deming Meng[1,2], Pei Wang[2], Jun Li[2], Jinlong Li[2], Yaodeng Chen[1], Steve Wangzong[2], Andy Heidinger[3], Andi Walther[2], and Zhenglong Li[2]

[1]Key Laboratory of Meteorological Disaster of Ministry of Education (KLME) / Joint International Research Laboratory of Climate and Environment Change (ILCEC) / Collaborative Innovation Center on Forecast and Evaluation of Meteorological Disasters, Nanjing University of Information Science & Technology, Nanjing, China, [2]Cooperative Institute for Meteorological Satellite Studies, University of Wisconsin-Madison, Madison, WI, USA, [3]Advanced Satellite Products Branch, NOAA/NESEDIS/STAR, Madison, WI, USA

Key Points:

- The NWP model background hydrometeors are used directly in the LWP and IWP operators by assuming water species partition ratios unchanged
- The LWP and IWP observations are successfully assimilated with the ability to propagate increments both horizontally and vertically
- The assimilation of LWP and IWP observations can improve the model prognostic variables accuracy, leading to better hurricane prediction

Correspondence to:
J. Li and Y. Chen,
jun.li@ssec.wisc.edu;
keyu@nuist.edu.cn

Citation:
Meng, D., Wang, P., Li, J., Li, J., Chen, Y., Wangzong, S., et al. (2021). New observation operators for cloud liquid/ice water path from ABI and their impact on assimilation and hurricane forecasts. *Journal of Geophysical Research: Atmospheres*, *126*, e2020JD034164. https://doi.org/10.1029/2020JD034164

Received 28 OCT 2020
Accepted 22 APR 2021

Abstract The cloud liquid/ice water path (LWP/IWP) can provide valuable information about the cloud and precipitation. For the first time, the Gridpoint Statistical Interpolation (GSI) system is applied to examine the impact of the high spatial and temporal resolution LWP and IWP products derived from the Advanced Baseline Imager (ABI) on the new generation geostationary environmental satellites (GOES-R series) in numerical weather prediction (NWP). To extend the GSI's capability to assimilate LWP and IWP products, a pair of new observation operators of LWP and IWP is developed to avoid the requirement for hydrometeor control variables. The new observation operators enable the direct use of hydrometeor background information from the NWP model and allow the vertical propagation of the water vapor increment according to the Jacobian distributions for the new LWP and IWP operators. The new LWP and IWP observation operators are evaluated by the single observation tests and the cycling assimilation and forecast experiments of Hurricane Irma (2017) and Hurricane Maria (2017). The results from single observation tests show that the assimilations of pseudo-LWP and pseudo-IWP can achieve positive water vapor increments, which also spread vertically according to the Jacobian distributions. The impact studies on two hurricanes demonstrate that the ABI LWP and IWP measurements can be successfully assimilated into the NWP model by the new observation operators, which enhances the water vapor analysis and further improves other atmospheric state variables in the forecast fields. The improved environmental fields lead to the overall forecast improvement for the two hurricanes, with the most notable track improvement.

Plain Language Summary Satellite data from the advanced baseline imager (ABI) onboard the new generation of the geostationary operational environmental satellite (GOES-R Series) can provide a large amount of valuable observation information under cloudy regions for numerical weather prediction (NWP). To make effective use of these observations, satellite-derived hydrometeor information, such as the cloud liquid water path (LWP) and cloud ice water path (IWP), can improve the forecasts. To effectively use the cloud information in NWP, a pair of new operators has been developed to use the hydrometeors (e.g., cloud, rain, ice) by assuming that the portion of each water species keeps the same as the background fields. The new operator can successfully assimilate the cloud products, enabling better use of moisture information in NWP from satellite measurements in cloudy regions. Hurricane Irma (2017) and Hurricane Maria (2017) studies demonstrate that track forecasts are improved by assimilating cloud products with the new operators.

1. Introduction

As powerful and deep tropical low-pressure systems, hurricane formation is always associated with cloud systems and precipitation, which is of large uncertainties caused by models' inability to correctly represent complex physical processes (Errico et al., 2007; Li et al., 2016). Therefore, hurricane forecast relies not only on a well-defined analysis of the environmental field in the clear sky area but also on providing an accurate initial field in the cloudy sky area. In addition to conventional observations, non-conventional observations

(e.g., radar and satellite) provide a wealth of multi-source observations for improving hurricane analysis under the cloudy skies.

The ongoing development of data assimilation methods allows scientists to conduct direct assimilation of satellite radiance data in cloudy areas to improve hurricane forecasts (e.g., Otkin, 2010, 2012; Yang et al., 2017; Zhu et al., 2016). For microwave sounder (MW) radiances, for example, the Hurricane Weather Research and Forecasting (HWRF) Model is updated to assimilate the all-sky radiances from the Advanced Technology Microwave Sounder (ATMS) by adding total condensate as a control variable and six hydrometeors as state variables (T. C. Wu et al., 2019). An empirical flow-dependent adaptive observation error inflation (AOEI) method and an adaptive background error inflation (ABEI) method within an ensemble Kalman filter are proposed for assimilating all-sky satellite brightness temperatures from the Advanced Baseline Imager (ABI) onboard GOES-16 (Minamide & Zhang, 2017, 2019). However, direct assimilation of cloudy infrared (IR) radiances is still challenging due to the nonlinearity of moist processes, the uncertainties of cloud microphysical variables, the uncertainties in radiative transfer models, and the mismatch in magnitude and location between the cloud observations and simulations (Geer et al., 2017; Kostka et al., 2014; Kurzrock et al., 2018; Li et al., 2016, 2017). Some alternative approaches are being proposed to assimilate the cloudy IR radiance. For example, the optimal cloud-clearing method is proposed to assimilate the cloud-cleared radiances to improve the hurricane forecast (Li et al., 2005; Wang et al. 2015, 2017).

To better initialize the hydrometeor variables in the numerical weather prediction (NWP) model, the assimilation of satellite cloud retrievals associated with model hydrometeors provides another alternative approach. It is more resource-friendly to assimilate the retrieved cloud products because the observation operators (maps the space of state variables into the space of observed state variables) for assimilating retrievals are more straightforward when compared with radiance assimilation (Migliorini, 2012). Efforts have been and are still being invested in deriving cloud properties from the satellite radiances. These cloud properties include cloud optical depth (COD) and cloud particle size (CPS), as well as liquid water path (LWP) and ice water path (IWP), both of which are derived from COD and CPS (Andi et al., 2013; Minnis et al., 2008, 2011; Walther et al., 2013; Walther & Heidinger, 2012). Among them, LWP and IWP, which are directly associated with the hydrometeors in the model, are assimilated in various ways to improve the initial hydrometeor fields of NWP. For example, the LWP and IWP from the Langley Research Center (LaRC) at National Aeronautics and Space Administration (NASA) (Minnis, 2007; Minnis et al., 2008) have been assimilated via different kinds of assimilation methods, including three-dimensional variational (3DVar), Ensemble Kalman filtering (EnKF), and hybrid method (Chen et al., 2015, 2016; Jones et al, 2013, 2015; Meng et al., 2019). Besides, T. C. Wu et al. (2016) have made beneficial attempts at developing the observation operators for integrated solid–water content (SWC) and liquid–water content (LWC) to assimilate the Tropical Rainfall Measuring Mission (TRMM)/GPM hydrometeor retrievals into the GSI data assimilation system specifically for hurricanes.

The ABI (Schmit et al., 2005, 2017) is a multi-channel passive imaging radiometer onboard the new generation of Geostationary Operational Environmental Satellite (R-Series) designed to observe the Western Hemisphere and provide various area imagery and radiometric information. ABI measures atmospheric or surface radiances in a total of 16 different spectral bands, including two visible (VIS) channels, four near-infrared (NIR) channels, and ten infrared (IR) channels with a minimum spatial resolution of 0.5 km. It observes the full disk every 10 min (mode 6), the continental United States (CONUS) every 5 min, and the mesoscale regions every 30 s. Compared with the previous generation of the GOES (8–15) imager, the spatial resolution and temporal resolution of the ABI are improved dramatically, benefiting the accuracy of the derived products (Goodman et al., 2020). The LWP and IWP, retrieved from the VIS band (channel 2) and the NIR band (channel 6), represent the amount of cloud water and cloud ice integrated from the surface to the top of the atmosphere. Compared with cloud products derived from other satellites or instruments, the LWP and IWP derived by ABI have a higher spatial resolution, with a spatial resolution of up to 2 km. Higher temporal and spatial resolutions provide more valuable information for NWP, especially for small-scale clouds.

The variational assimilation of LWP and IWP products highly relies on the hydrometeor control variables. It is relatively straight forward to test the hydrometeors impacts with the established LWP and IWP operators within the data assimilation systems that contain the hydrometeors control variable, such as the Weather

Research and Forecasting (WRF) model's Data Assimilation System (WRFDA) (Chen et al., 2015, 2016; Jones et al., 2013, 2015). Unfortunately, there is a lack of hydrometeors control variables in some of the data assimilation systems, for example, the Gridpoint Statistical Interpolation (GSI) system, which is an operation-based assimilation system. GSI has a good capability to assimilate varieties of satellite observations and is widely used in operational center (e.g., Kleist et al., 2009; Zhu et al., 2016) and research community (e.g., Lee et al., 2019; Wang et al., 2015; Wu & Zupanski, 2017). The observation operators for integrated SWC and LWC in GSI system were developed by T. C. Wu et al. (2016). The observation operators are built based on the assumption that super-saturated water vapor will condense out immediately. Hydrometeor control variables are then not required since the assumption only depends on temperature, specific humidity, and pressure. The hydrometeors species in the background are calculated by an empirical formula instead of being diagnosed by the microphysical parameterization scheme. However, as pointed out by T. C. Wu et al. (2016), a portion of supersaturated water vapor used in the SWC&LWC operator has been condensed by the model microphysics and/or cumulus parameters. Thus, the simulated background of hydrometeors may have a negative bias. The SWC and LWC operators are further improved by using the hydrometeor species estimated from the HWRF microphysics directly and including total cloud condensate (CWM) as a control variable (Wu & Zupanski, 2017). In their study, the individual hydrometeors are diagnosed from CWM and the partition parameters that include the fraction of ice (F_ICE), the fraction of rain (F_RAIN), and values of riming rate (F_RIMEF). But these variables only exist in the Nonhydrostatic Mesoscale Model (NMM) core of the Weather Research and Forecasting (WRF), which cannot be found in the Advanced Research WRF (WRF-ARW) model.

Since the output of the WRF-ARW model contains the hydrometeor variables [including liquid water mixing ratio (Q_{cloud}), ice water mixing ratio (Q_{ice}), rainwater mixing ratio (Q_{rain}), snow water mixing ratio(Q_{snow}), and graupel mixing ratio (Q_{graup})] by the diagnostics from microphysical parameterization, it is better to define the cloud-related operators using the hydrometeor variables directly. Two issues need to be addressed to achieve this goal: (1) How to relate the hydrometeor variables to the water vapor, which is the control variable of the GSI; (2) How to distribute the LWP and IWP vertically in each model grid since the observation only provides the column-integrated water and ice in the horizontal atmosphere. Similar works have been conducted in Yucel et al. (2002, 2003) where they assimilated the high-resolution remotely sensed cloud cover into the Regional Atmospheric Modeling System (RAMS) and the fifth-generation Pennsylvania State University–National Center for Atmospheric Research (PSU–NCAR) Mesoscale Model (MM5). In their studies, RAMS and MM5 are assumed to correctly characterize the relative proportions of different cloud species but not necessarily the total amount of cloud water/ice. The direct replacement or nudging assimilation technique is applied in their studies to update the cloud microphysics. In this study, new LWP and IWP observation operators have been developed based on the same assumption that the WRF-ARW model correctly characterize the relative vertical position of each water species and the relative proportions of each water species in a variational assimilation method. Thus, the ratio of each water species to its sum at the 3D grid point is directly obtained from the NWP model and remains constant during the iterative process.

The structure of this paper is organized as follows: Section 2 describes the cloud products derived from ABI radiance measurements. Section 3 explains in details the methodology for the new LWP and IWP observation operators. The validation of the LWP and IWP observation operators is presented in Section 4. Section 5 presents the ABI LWP and IWP data impacts on the analysis and forecasts for two typical hurricane cases. A summary is given in Section 6.

2. Hurricane Cases and ABI LWP and IWP Data

Two hurricanes cases The daytime cloud optical and microphysical properties (DCOMP) algorithm from the GOES-R series Algorithm Working Group (AWG) generates the daytime cloud products from the imagery taken by the ABI onboard GOES-16/-17 (Walther et al., 2013; Walther & Heidinger, 2012) for every pixel classified as cloudy. Only daytime pixels are considered because VIS and NIR channels are simultaneously used in the microphysical property retrievals. The "daytime" pixels are defined by the solar zenith angle less than or equal to 65°. The cloud masks provided by the ABI Cloud Mask (ACM) algorithm are used to determine the cloudy or cloud-free pixel. Besides, the cloud top pressure and cloud phase (CP) from other

ABI/GOES-R retrievals are also required. Details on the DCOMP algorithm can be found in the DCOMP Algorithm Theoretical Basis Document (ATBD; Andi et al., 2013).

The microphysical properties include COD, CPS, LWP, and IWP, among others. The LWP and IWP, retrieved from the VIS band (channel 2) and the NIR band (channel 6), represent the amount of cloud water and cloud ice integrated from the surface to the top of the atmosphere. There are 5424 scan lines for ABI VIS and NIR bands, each of which has 5424 pixels. The LWP and IWP are stored at each pixel with spatial and temporal resolutions of 2 km at nadir and 30 min, respectively. Each cloud pixel is identified as either an ice phase or a liquid phase based on the CP look-up table (LUT; Michael et al., 2010). The cloud information reflected by LWP and IWP is different. The COD at the VIS wavelengths can be converted to IWP for optically thin clouds, which are mostly non-precipitating (Ebert & Curry, 1992; Lin & Rossow, 1996; Wang & Sassen, 2002). With both VIS and NIR radiance measurements, the COD and the CPS in the radius are first retrieved, and further leads to the LWP retrieval for boundary layer clouds (Bennartz et al., 2007) that are likely both precipitating and non-precipitating. The different observation information responds to different observation operators, which will be described in detail in Section 3.2.

The ABI cloud products (unit: kg/m^2) are compared with the Global Geostationary Gridded Cloud (G3C) products from the NASA Langley Cloud and Radiation Research Group (Minnis, 2007; Minnis et al., 2008) for a qualitative check. The G3C products also include LWP and IWP (unit: kg/m^2), which can be used as references for ABI cloud products. The hourly available G3C products are averaged on a uniform grid of 0.25°latitude by 0.3125°longitude. The maps of both ABI-derived cloud products and G3C products are shown in Figure 1. The spatial distributions of the LWP and IWP measurements from ABI are similar to those from G3C. The IWP from both G3C products (Figure 1a) and ABI-derived products (Figure 1b) capture the main structural characteristics of the hurricane spiral bands. Whereas the LWP data from G3C (Figure 1c) and ABI (Figure 1d) primarily provide cloud observations in environmental fields. For both the ABI and G3C derived products, the magnitude of IWP is larger than the magnitude of LWP since high ice clouds always dominate the strong convective weather phenomena, such as in the hurricane area. Besides, there is more detailed information from the ABI-derived LWP and IWP data due to the higher horizontal resolution, which should benefit the NWP model initialization.

3. Methodology for Assimilating ABI-Derived LWP and IWP

Since the hydrometeors are not included in control variables in the current GSI system (GSI v3.7; W. S. Wu et al., 2002), it is crucial to obtain the proxy of hydrometeor species and to update the proxy during the assimilation process. The LWP and IWP observation operators can then be derived based on the hydrometeor proxy. Besides, due to the LWP and IWP only provides information on the horizontal cloud observations, a method is needed to define the vertical propagation of the cloud information to the model.

3.1. The Proxies for Background Hydrometeor Species

The relationship needs to be established between hydrometeors and Q_v, that is, Q_v is used as a proxy for hydrometeors. In this study, the WRF-ARW output, which is used as the background fields for GSI, contains all needed water species such as Q_v, Q_{cloud}, Q_{ice}, Q_{rain}, Q_{snow}, and Q_{graup}, which represent the mass mixing ratios over dry air (unit: kg/kg). Inspired by the strategies of updating model cloud microphysical based on satellite images (Yucel et al. 2002, 2003), it is assumed that the models correctly calculate the partitions of different water species at each model grid point, even though their magnitudes may be incorrect. The proportion of each water species at each grid point in the model is assumed to be constant during the iterations. The total water vapor (Q_t) at each grid point, representing the sum of all water species, is calculated first from the background field based on the following equation:

$$\begin{cases} Q_t^k = Q_v^k + Q_{hydro}^k \\ Q_{hydro}^k = Q_{cloud}^k + Q_{ice}^k + Q_{rain}^k + Q_{snow}^k + Q_{graup}^k \end{cases} \quad (1)$$

where k denotes the model level index, Q_v^k stands for water vapor at the k_{th} level, and Q_{hydro}^k stands for hydrometeor species, including $Q_{cloud}^k, Q_{ice}^k, Q_{rain}^k, Q_{snow}^k$, and Q_{graup}^k at the k_{th} level.

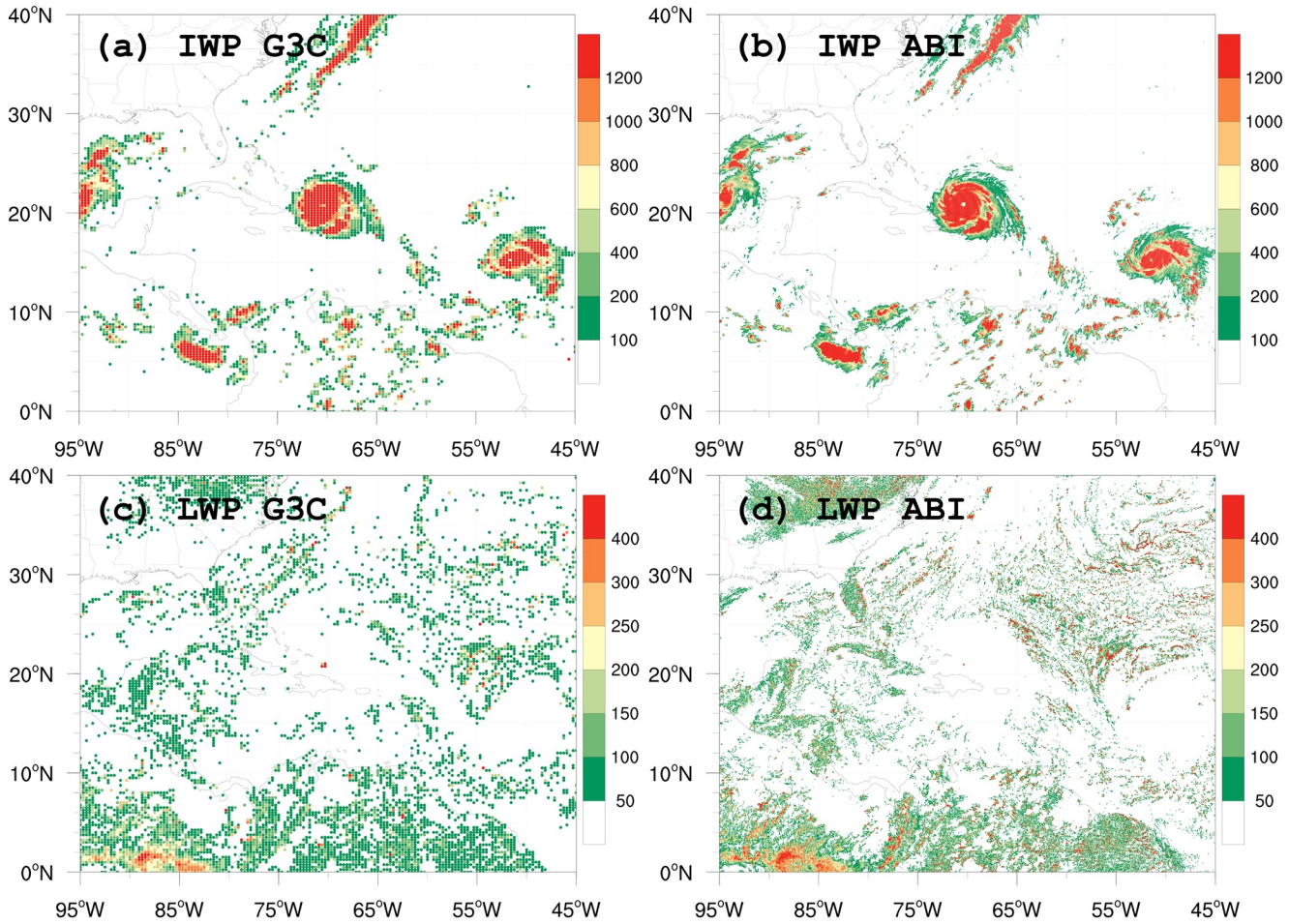

Figure 1. The distribution of (a), (b) Ice Water Path (IWP) and (c), (d) Liquid Water Path (LWP) for (a), (c) G3C, and (b), (d) ABI-derived cloud products at 1800 UTC 06 September 2017 during Hurricane Irma (2017). The unit is g/m^2 for both LWP and IWP.

Recall that Q_v^k is one of the control variables in GSI (W. S. Wu et al., 2002), which can be updated during the iteration. To obtain Q_t^k, the ratio between Q_v^k and Q_t^k at each grid in the model field needs to be calculated, and remains constant during the iteration,

$$R_{vapor}^k = \frac{Q_v^k}{Q_t^k} \tag{2}$$

Simultaneously, the ratios between hydrometeor species Q_{hydro} and Q_t at each grid in the background field are also calculated before the iteration and remains unchanged during the iteration,

$$R_{hydro}^k = \frac{Q_{hydro}^k}{Q_t^k} \tag{3}$$

Therefore, in the outer loop iterations, the hydrometeors species at the k_{th} level can be obtained once the Q_v^k is updated,

$$Q_{hydro}^k = \frac{Q_v^k}{R_{vapor}^k} \cdot R_{hydro}^k \tag{4}$$

It can be seen from Equation 4 that Q^k_{hydro} can only be obtained when the R^k_{hydro} is larger than 0. In other words, LWP and IWP can only be assimilated where both the background and the observation are defined as cloudy. In this way, even though the current data assimilation system does not contain the hydrometeor control variables, it is possible to obtain the hydrometeor proxies in the iterative process under the assumption of unchanged water species partition ratios. These hydrometeor proxies can be used to construct the corresponding observation operators during the subsequent assimilation process.

3.2. LWP and IWP Observation Operators

As discussed in Section 2.2, the ABI-derived IWP represents the non-precipitating cloud, while the ABI-derived LWP contains both precipitating and non-precipitating information. Therefore, the variables chosen for the LWP and IWP operators may differ from each other. In the WRF-ARW model, the non-precipitable and precipitable clouds can be represented by lower-level hydrometeors, that is, Q_{cloud} and Q_{rain}, respectively, while the non-precipitating ice cloud can be represented by higher-level hydrometeors, that is, Q_{ice} (Hong & Lim, 2006). LWP and IWP measurements reflect the column-integrated water and ice in the atmosphere, respectively, which represents the vertical cumulative sum of liquid water cloud and ice water cloud. The LWP and IWP observation operators should be constructed in the same way, integrating the simulated liquid and ice-phase clouds in the whole atmosphere, respectively. Similar construction schemes can be found in previous studies (Chen et al., 2015, 2016; Jones et al., 2013, 2015; Wu & Zupanski, 2017). Thus, the observation operators for LWP (H_{liquid}) and IWP (H_{ice}) from GOES-16 series ABI cloud products are

$$\begin{cases} H_{liquid} = \sum\limits_{k=1}^{k_{\max}} Q^k_{liquid} \cdot \dfrac{\Delta P^k}{g} = \sum\limits_{k=1}^{k_{\max}} \left(\dfrac{Q^k_v}{R^k_{vapor}} \cdot R^k_{liquid} \right) \cdot \dfrac{\Delta P^k}{g} \\ H_{ice} = \sum\limits_{k=1}^{k_{\max}} Q^k_{ice} \cdot \dfrac{\Delta P^k}{g} = \sum\limits_{k=1}^{k_{\max}} \left(\dfrac{Q^k_v}{R^k_{vapor}} \cdot R^k_{ice} \right) \cdot \dfrac{\Delta P^k}{g} \end{cases} \tag{5}$$

where Q^k_{liquid} (unit: kg/kg) is the sum of Q^k_{cloud} and Q^k_{rain} and Q^k_{ice} (unit: kg/kg) denotes the non-precipitating ice cloud. R^k_{liquid} and R^k_{ice} are the ratios between liquid/ice water and Q^k_t at the k_{th} level and are calculated for Q^k_{liquid} and Q^k_{ice}, respectively, k_{max} is the index for the model top level. ΔP^k $\left(\text{unit}: \text{hPa}\right)$ is the pressure gradient between levels k and $k+1$ ($k \le k_{max}-1$), and g $\left(\text{unit}: \text{m}/s^2\right)$ denotes to the acceleration due to gravity. It should be noted that the complicated microphysical processes involved in hydrometeors condensation have been considered in detail by the microphysics parameterization and cumulus parameterization scheme, including the special situation such as supercooled water, where ice and liquid clouds coexist. Therefore, the H_{liquid} and H_{ice} are calculated by integrating the hydrometeor proxies into the whole levels to ensure consistency with the model field.

Besides, the derivatives of the operators with respect to Q_v (often referred to as Jacobians) are also calculated

$$\begin{cases} \dfrac{\partial H_{liquid}}{\partial Qv} = \dfrac{R^k_{liquid}}{R^k_{vapor}} \cdot \dfrac{\Delta P^k}{g} = \dfrac{Q^k_{liquid}}{Q^k_v} \cdot \dfrac{\Delta P^k}{g} \\ \dfrac{\partial H_{ice}}{\partial Qv} = \dfrac{R^k_{ice}}{R^k_{vapor}} \cdot \dfrac{\Delta P^k}{g} = \dfrac{Q^k_{ice}}{Q^k_v} \cdot \dfrac{\Delta P^k}{g} \end{cases} \tag{6}$$

The Jacobians of H_{liquid} and H_{ice} quantifies the sensitivities of the hydrometers to Q_v. Equation 6 shows that the Jacobians of the LWP and IWP observation operators are related to the ratios of water species in the model fields and the variation in pressure. Furthermore, the Jacobians also define how the increments of LWP and IWP assimilation with the new LWP and IWP observation operators propagate vertically, that is, according to the ratios between hydrometeors and water vapor at the corresponding vertical levels.

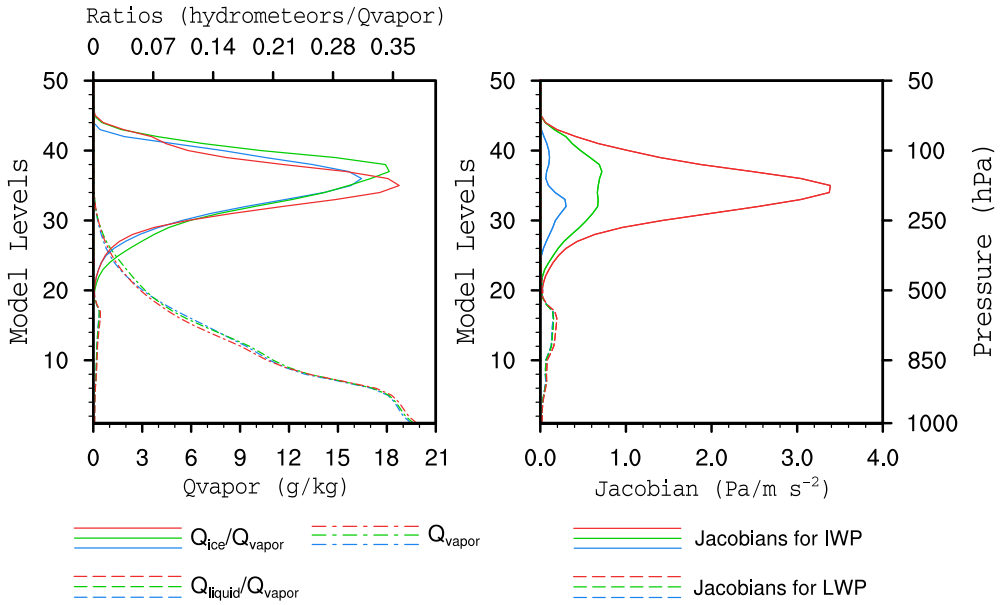

Figure 2. (a) The vertical distribution of water vapor (dash dotted lines), and the ratios between liquid (dash lines)/ice (solid lines) cloud and water vapor. (b) The vertical distribution of the Jacobians functions for the LWP (dash lines) and IWP (solid lines). The results are for 1800 UTC 06 September (blue lines), 1800 UTC 07 September (green lines), and 1800 UTC 08 September (red lines) averaged over the hurricane core area.

4. Analysis and Test of New LWP and IWP Operators

4.1. Jacobians for the New LWP and IWP Operators

Three analysis fields are used to show the Jacobian distributions for the new LWP and IWP operators. It is shown in Equation 6 that the final form of Jacobians consists of two parts: (1) the ratios between the hydrometeors and water vapor and (2) the pressure gradient term $\frac{\Delta P^k}{g}$. The patterns of the vertical distributions of water vapor and the ratios (Figure 2a) are similar among the three analysis times. The water vapor content gradually decreases as altitude increases. In the lower and middle troposphere, the ratios of the liquid cloud to water vapor are small, while the ratios between ice clouds and water vapor increase due to the decrease in water vapor in the higher altitudes. In general, the patterns of ratios are relatively stable over this period. However, the Jacobians (Figure 2b) show different vertical distribution characteristics, especially for the IWP. From 1800 UTC 06 to 1800 UTC 08 September, the magnitude of Jacobians gradually increases, which is related to the pressure variation of Hurricane Irma (2017). The pressure gradients in the vertical layers are enhanced, which in turn contributes to the magnitude changes of the Jacobians.

Additionally, the Jacobian vertical distributions also show the sensitivity of the new LWP and IWP observation operators to water vapor. The new LWP operator reveals high sensitivity of LWP to water vapor in the lower layers, while the new IWP operator reveals high sensitivity of IWP to water vapor in the middle and upper troposphere. That means although the observations of LWP and IWP from ABI are the column integration of the cloud, the increments in the assimilation of LWP and IWP would propagate to water vapor vertically according to the corresponding Jacobians, respectively.

4.2. Single Observation Tests

To validate the new LWP and IWP observation operators, a set of single observation tests is conducted. The background fields used for the single observation tests are from 1800 UTC 6 September 2017, which were generated from a 6-h WRF forecast. A pseudo-LWP observation and a pseudo-IWP observation are placed at the hurricane center (17.5°N, 66°W) with the innovations (observation minus background) of 1000 g/m^2, respectively. The observation errors are assigned to 500 g/m^2 for both LWP and IWP for assimilation. The

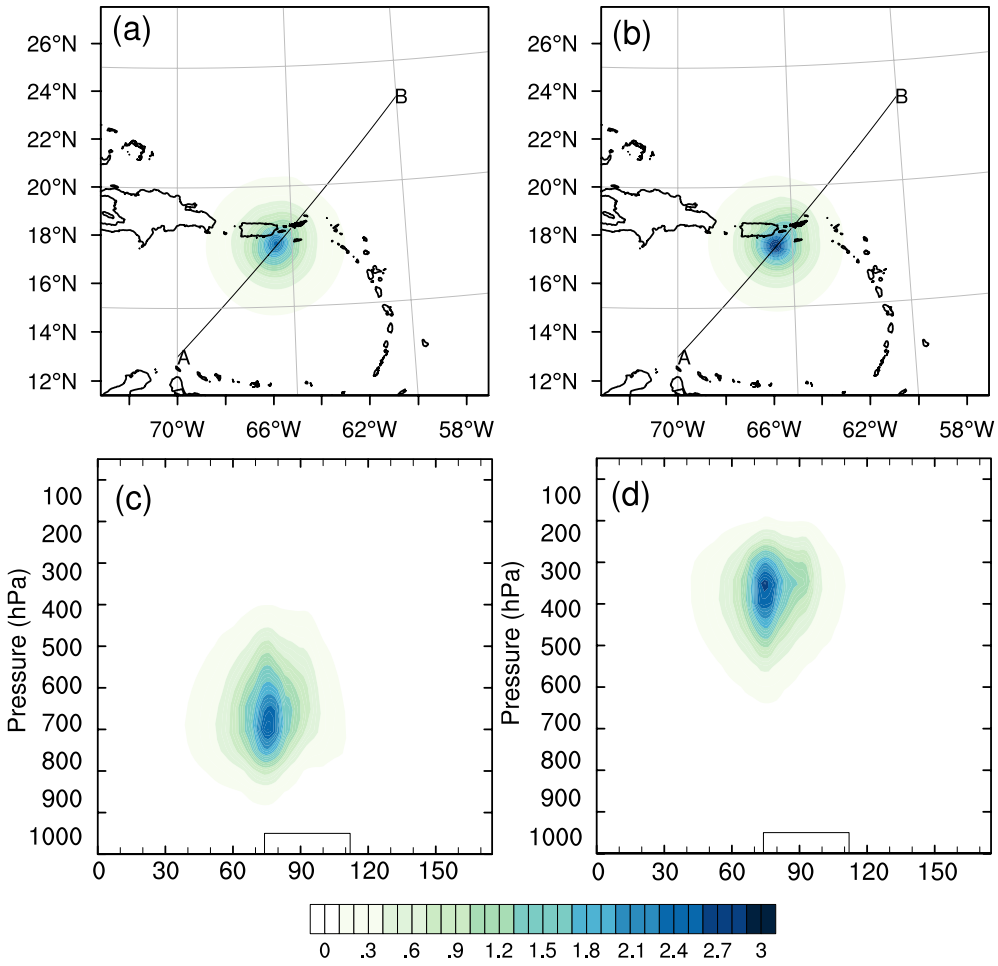

Figure 3. The increments of water vapor (unit: kg/kg) at (a) 700 and (b) 300 hPa after assimilating single pseudo-LWP and pseudo-IWP, respectively. Their cross sections along the line from A point to B point are presented in (c) and (d), respectively.

new LWP and IWP operators use specific humidity as the control variable. Figure 3 shows the increments of water vapor in the analysis fields (unit: kg/kg). The positive water vapor increments are observed at around 700 and 400 hPa with respect to the assimilation of pseudo-LWP (Figure 3a) and pseudo-IWP (Figure 3b). The increment of water vapor is stronger with the assimilation of the pseudo-IWP data than the increment of water vapor with the assimilation of the pseudo-LWP data. This is because the magnitude of the Jacobians for IWP in the new LWP & IWP operators is larger than that of the Jacobians for LWP. Cross section along the line from A point to B point shows that the increment from the assimilation of pseudo-IWP occurs mainly in the upper level with a center at around 350 hPa, while the increment from the assimilation of pseudo-LWP is concentrated below 500 hPa with a center at around 700 hPa. The vertical propagation of the water vapor increment results from the Jacobian changes in the vertical direction.

5. Impacts of the New LWP and IWP Operators on Hurricane Forecast

Continuous cycling data assimilation and forecast experiments for Hurricane Irma (2017) and Hurricane Maria (2017) are carried out to evaluate the impact of the new LWP and IWP operators on the hurricane cases.

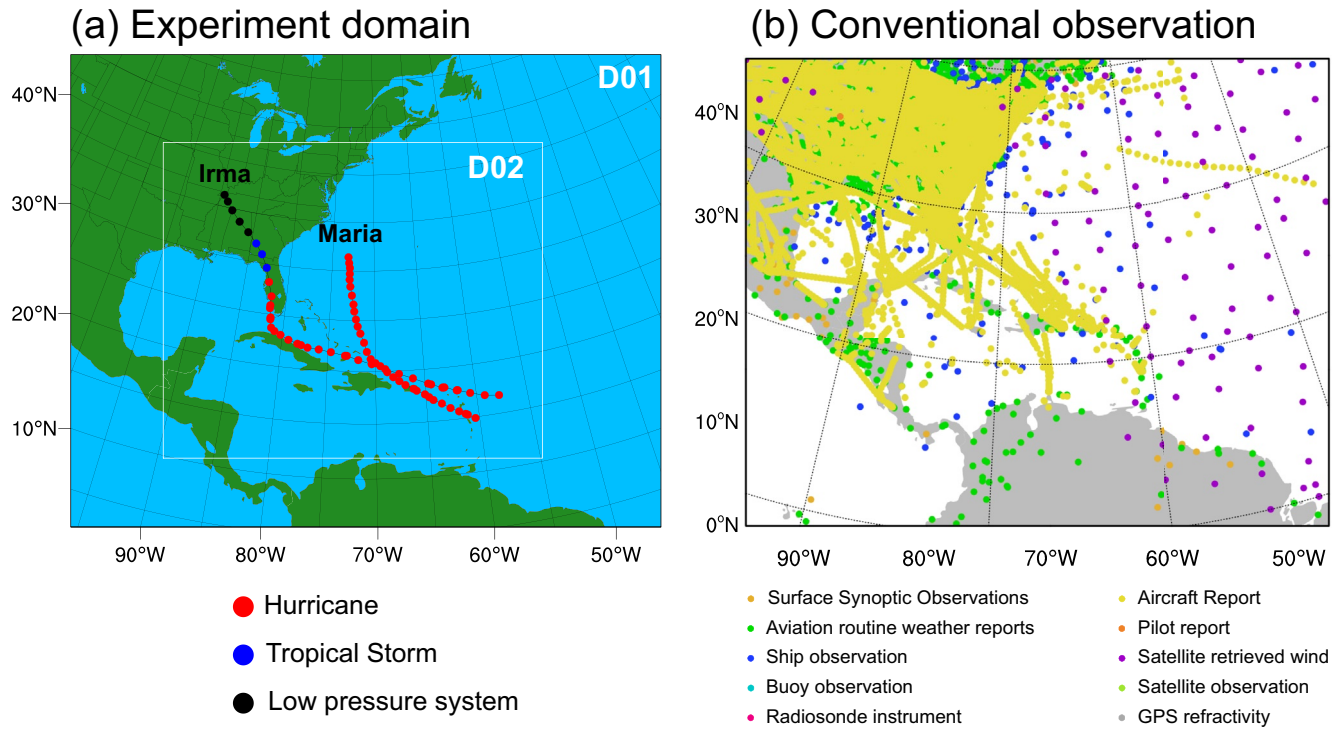

Figure 4. (a) The 27/9-km nested domains for data assimilation and forecast experiments. (b) The distribution of conventional observations in D01 assimilated in this study valid at 1800 UTC 06 September 2017.

5.1. Models and Experimental Design

The Developmental Testbed Center (DTC; Bernardet et al., 2008) GSI version 3.7 is used as the data assimilation system with the WRF-ARW as the NWP model. The GSI three-dimensional variational data assimilation (3DVar) method is used with a homogeneous background covariance matrix (W. S. Wu et al., 2002). Control variables include stream function, velocity potential, pressure, and a humidity variable (specific or relative humidity). The background error covariance comes from the North American Mesoscale Forecast System (NAM) regional model. The new LWP and IWP operators have been implemented in the GSI system. The National Centers for Environmental Prediction (NCEP) FNL (Final) operational global analysis (0.25°×0.25°) are used as the initial and boundary fields. The nested domain is used in Lambert Projection with the corresponding horizontal grid spacing as 27 and 9 km, respectively. There are 250 × 200 grid points in the outside domain (D01) and 481 × 400 grid points in the inner domain (D02) with the central latitude and longitude at (22°N,77°W) (Figure 4a). The model is configured with 51 vertical levels and a 50 hPa model top. Besides, the sea level temperature (SST) dataset comes from the FNL dataset. It should be noted that moving nested domain is used as efficient forecasting tools for hurricane predictions, especially valuable for the characterization of hurricane structures (Biswas et al., 2014; Li et al., 2020; Tong et al., 2018). This study focuses on testing the effectiveness of the LWP and IWP observation operators instead of hurricane refinement structure diagnosis. Therefore, a larger fixed domain (D02) is needed to cover the tracks of both hurricanes, provide a better environmental field for hurricane simulations, and enable more LWP and IWP observations to be assimilated. Based on the above considerations, 27 km nested with 9 km domains are chosen by referring to HWRF horizontal grids setup but without the third layer moving domain used.

Since the new LWP and IWP operators are constructed by using the hydrometeors directly, it is sensitive to the choice of microphysics scheme. To select an optimal microphysical parameterization scheme for LWP and IWP assimilation, several microphysics schemes are selected to test the sensitivity of the new LWP and IWP operators, including WRF Single-Moment 6-Class Microphysics Scheme (WSM6), the WRF Double Moment 6-class (WDM6) scheme, Lin scheme, Thompson scheme, Morrison double-moment scheme. Kain-Fritsch scheme (KF) is adopted as cumulus parameterization scheme. Sensitivity experiments are

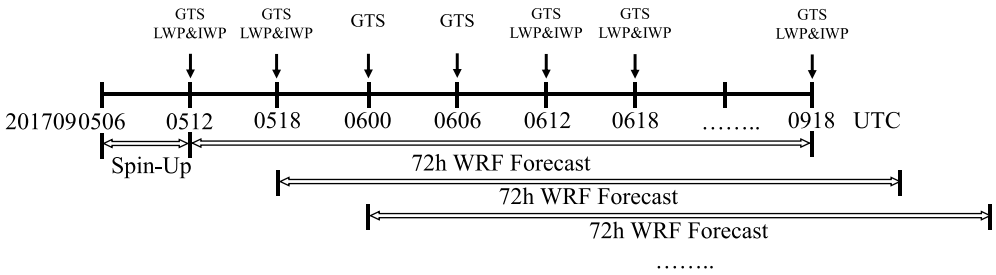

Figure 5. Flow charts of the cycling data assimilation experiments for Hurricane Irma (2017). The background field for each analysis is taken from the 6-h forecast of the previous cycle. The same for Hurricane Maria (2017) but with start time at 1200 UTC 18 September 2017 and end time at 1800 UTC 22 September 2017.

evaluated based on three LWP and IWP assimilation and forecast results, beginning at 1800 UTC 5 September 1800 UTC 6 September, and 1800 UTC 7 September 2017, respectively, with background fields from 6 h forecast fields after the 1200 UTC cold start for each day. Overall, the average track errors and intensity errors (not shown) show that the WSM6 parameterization scheme has the smallest errors in all experiments. Therefore, WSM6 and KF are adopted as the microphysics scheme and cumulus parameterization scheme, respectively. Other parameterizations include the Yonsei University boundary layer scheme (YSU; Hong et al., 2006), the Dudhia shortwave radiation scheme (Dudhia, 1989), and the Rapid Radiative Transfer Model (RRTM) longwave radiation scheme (Mlawer et al., 1997).

Two experiments are conducted to examine the performance of the new LWP and IWP observation operators. The first one is the control experiment (hereafter *CNTL*) using the released version of GSI without any modifications, which is only assimilating the conventional observations from radiosondes, ships, aircraft reports, satellite-derived winds, surface synoptic observations, and airport reports for both D01 and D02 (Figure 4b). As a comparison, the second experiment additionally assimilates the LWP and IWP data derived from ABI/GOES-16 with the new LWP and IWP operators incorporated into GSI version 3.7, which takes the advantages of the hydrometeor information from the model (referred as *Hydro*). The LWP and IWP are only assimilated for D02. Accounting for the 9 km grid resolution and the horizontal length scale of the control variable Q_v, LWP and IWP are thinned by 20 km (about 2 times the grid). The observation errors are estimated following Desroziers et al., 2005, using both $O - B$ (observation minus background) and $O - A$ (observation minus analysis). In this study, the constant with the values of 300 g/m^2 is assigned to both LWP and IWP. It is worth noting that scenario-dependent observation error assignments (e.g., defined as a function of LWP and IWP values) need to be further investigated to obtain better LWP and IWP analysis, which will be carried out in the future study. The quality control (QC) application in this study is the default gross check function in GSI, which is also used in many other studies (e.g., Gasperoni, et al., 2020; Li et al., 2020; T. C. Wu et al., 2019). It eliminates observations that differ from the background by more than three times the observation error.

In both *CNTL* and *Hydro* experiments, a total of 18 cycling analyses for Hurricane Irma (2017) from 0600 UTC 05 September 2017, to 1800 UTC 09 September 2017, and 17 cycling analyses for Hurricane Maria (2017) from 1,200 UTC 18 September 2017, to 1,800 UTC 22 September 2017, are conducted with a 6-h spin-up run before the first analysis (Figure 5). 72-h forecasts are made after each assimilation. It should be noted that the LWP and IWP data are retrieved from the VIS band radiances, which are only available during daytime, that is, 1200 UTC and 1800 UTC.

5.2. Verification Against the LWP and IWP Observations

To evaluate the impacts of the new LWP and IWP operators on the analyses and forecasts in the cycling data assimilation, the LWP and IWP data number, the mean bias, and the standard deviation (STD) of the model versus observations are presented in Figure 6 for Hurricane Irma (2017). It shows that the number of assimilated IWP data varies with time (Figure 6a) due to the effects of daytime coverage. The average utilization percentage of the observations is around 30%, and observations that differ significantly from the background field are eliminated during QC. For example, the differences between observations and background are larger than three times the observation error, or the background is defined as clear sky. IWP

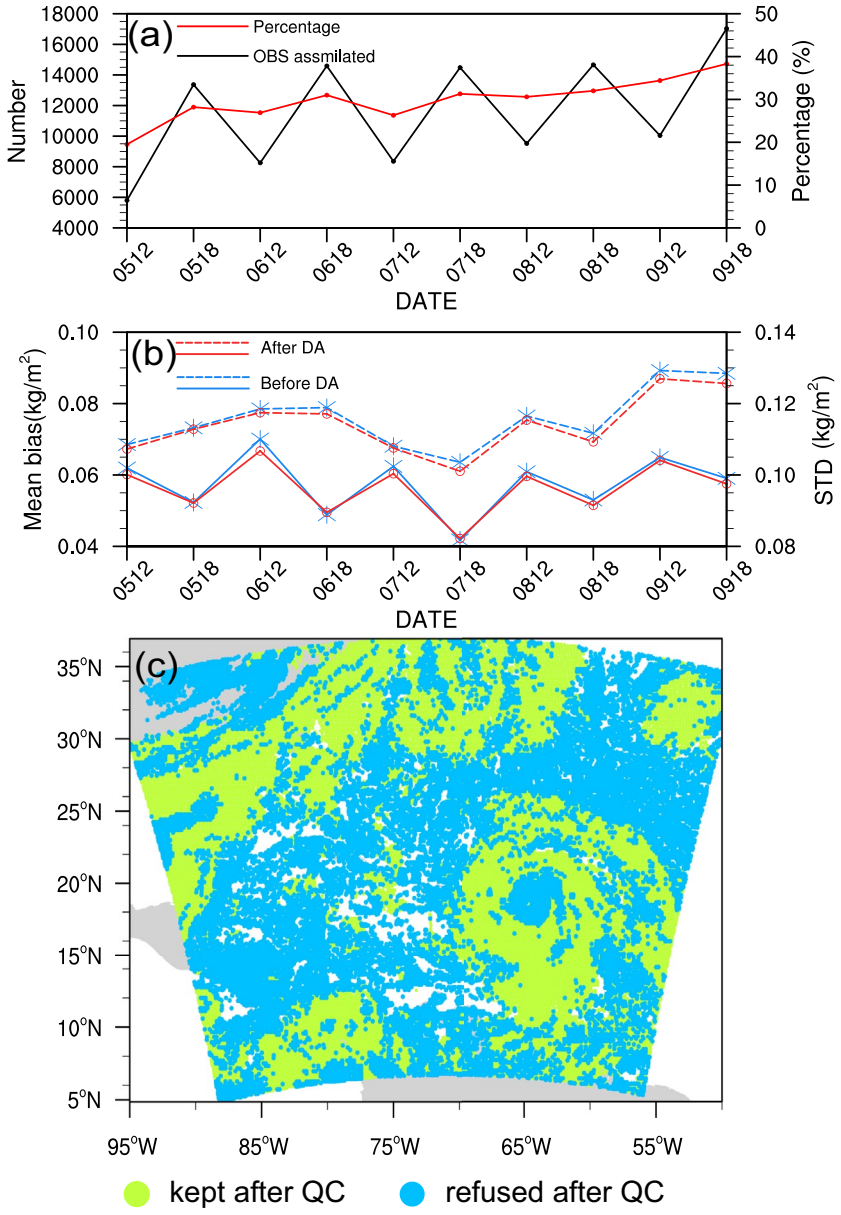

Figure 6. (a) Time series of the number of IWP and LWP observations used in assimilation (black line) and the utilization percentage (red line), (b) mean bias against the observed LWP and IWP (solid lines) and standard deviation against the observed LWP and IWP (dashed lines) before (blue lines) and after (red lines) data assimilation (DA), (c) the kept and refused LWP and IWP observation distribution after QC.

has a higher utilization rate than LWP. This is because the simulated liquid clouds are mainly located in the convective area, but the LWP observations are mostly distributed in the hurricane environments, where it is defined as clear sky by the model. Therefore, the majority of the LWP in hurricane environments is eliminated. Figure 6c shows an example at 1800 UTC 06 September 2017 for Hurricane Irma (2017) that the LWP and IWP are assimilated or rejected. Observations in the hurricane environments and in the strong convective areas are both removed. It is worth noting that the rejected observations may have significant biases and differ too much from the background, and the assimilation of these products may severely damage the model performance.

Based on these assimilated observations, mean bias and STD are calculated. For the mean bias (Figure 6b solid lines), it is clear that the assimilation of the LWP and IWP data can consistently reduce the mean bias

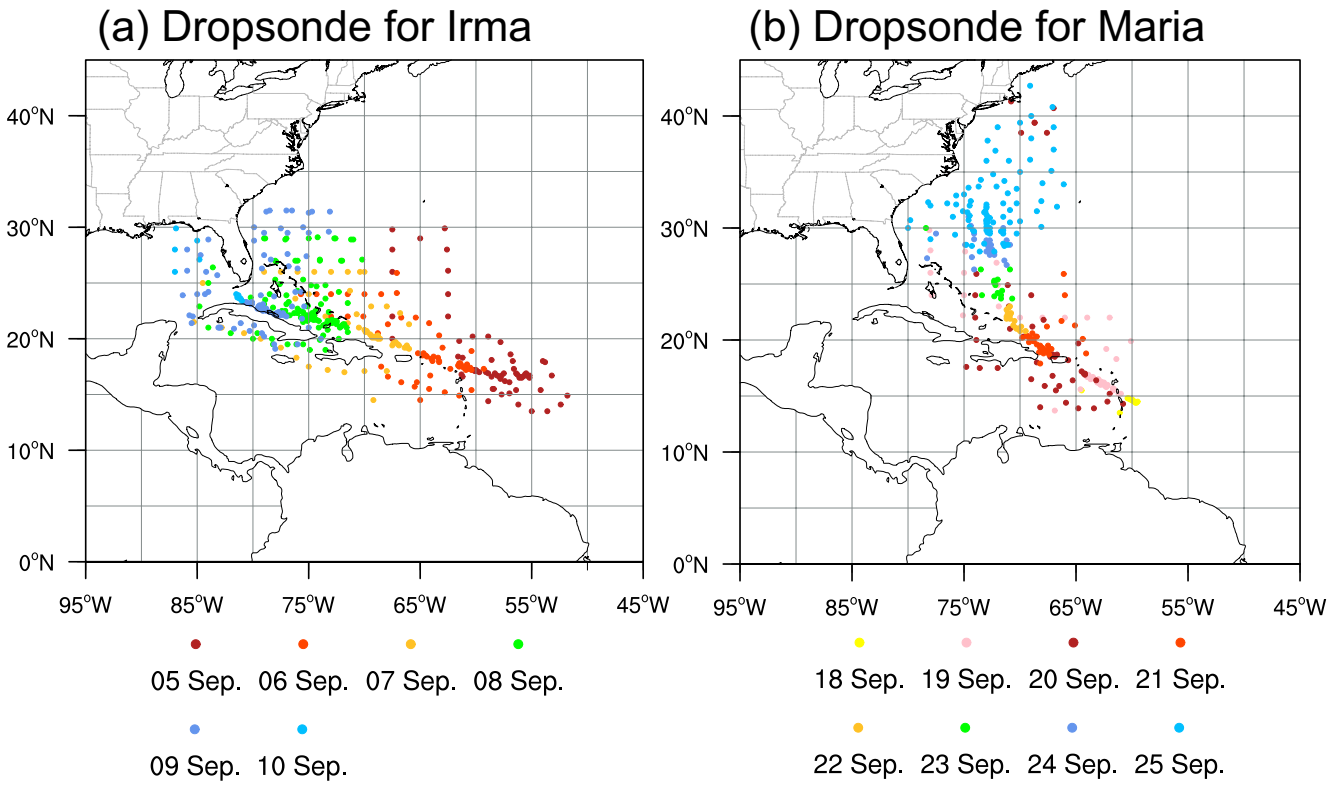

Figure 7. The distribution of dropsonde soundings observations from the National Hurricane Operations Plan (NHOP) for (a) Irma case and (b) Maria case. The numbers in the legend are dates in September 2017.

with an average reduction of 1.8%, indicating that the new LWP and IWP operators effectively assimilate the LWP and IWP data at all analysis times. Moreover, the STD (Figure 6b dashed lines) after assimilation is also smaller than that before assimilation with an average reduction of 1.4%, meaning that the variations of the differences between the observed and the simulated LWP and IWP decrease with the assimilation of LWP and IWP data. As we can see, the improvement of the mean deviation and STD is small, which can be attributed to two reasons. First, the observations used to improve the model are limited, and the LWP and IWP observations in the hurricane core area are eliminated by QC; second, the background error covariance used here is designed for water vapor, which needs to be better characterized for hydrometeors. Although the improvement is small, assimilating the LWP and IWP using the new observation operators does reduce the bias and STD. These results are expected since when the LWP and IWP are assimilated using the new operators, the water vapor in the analysis field is improved, and thus, the simulated LWP and IWP from the model can better fit the observations.

5.3. Verification Against the Dropsonde Soundings

The independent sounding observations obtained from the National Hurricane Operations Plan (NHOP) are used to verify the impact of the new LWP and IWP operators on both hurricanes analysis and forecast. NHOP is published annually before the hurricane season, with the objective of providing forecasts, warnings, and assessments concerning tropical and subtropical weather systems for the United States and designated international recipients (Landsea & Franklin, 2013; OFCM 2017; Rappaport et al., 2009; Sanabia et al., 2013; Vonich & Hakim, 2018). The distributions of dropsonde observations are shown in Figure 7. The sounding observations cover the entire lifetime of Hurricane Irma (2017) and Hurricane Maria (2017).

The root means square error (RMSE) is used for the verification metrics for four variables, that is, the zonal (U) and meridional (V) components of wind, temperature (T), and specific humidity (Q), which is calculated by the following equation

$$RMSE = \sqrt{\frac{1}{N}\sum_{i=1}^{N}\left(X_{obs,i} - X_{model,i}\right)^2} \quad (7)$$

where N represents the total observation number, X_{obs} is the observations obtained from NHOP, and X_{model} is the model variable that interpolated to the observation space. The calculation is performed through the Model Evaluation Tools (MET) developed by DTC, which matches model outputs and observations in different spatial and time spaces together.

Figure 8 reveals the vertical profiles of RMSE for the analysis, 12-h forecast, and 24-h forecast fields for Hurricane Irma (2017). There is little difference of RMSE above 500 hPa and at the sea surface between the two experiments, especially for U and V wind fields. The analysis field of the U wind field (Figure 8a) has

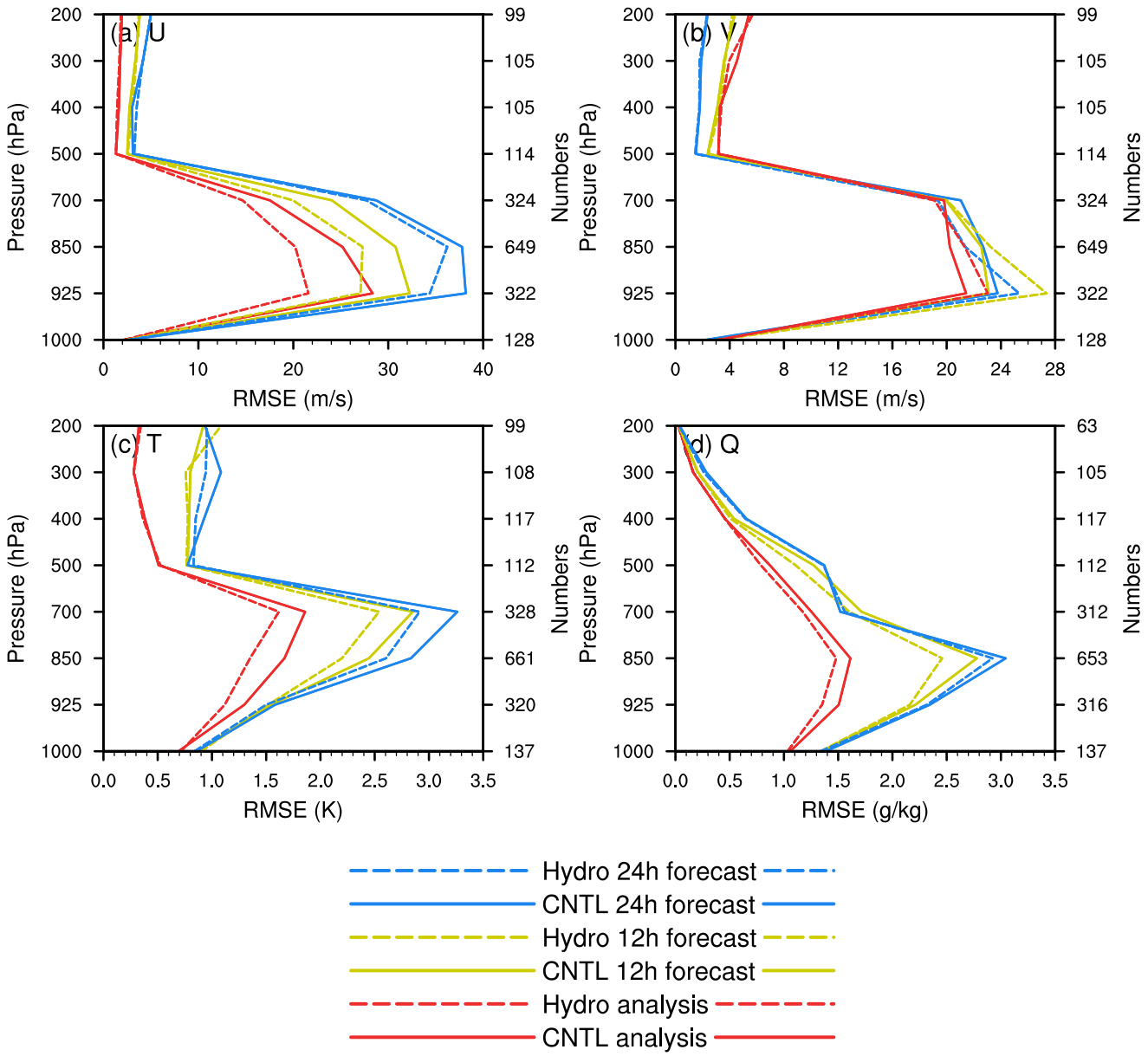

Figure 8. Vertical profiles of the analysis (red lines), 12 h forecast (yellow lines), and 24 h forecast (blue lines) RMSE for Hurricane Irma (2017) of (a) U (m s^{-1}), (b) V (m s^{-1}), (c) T (k) and (d) Q (g/kg) compared with the independent dropsonde sounding observations obtained from the National Hurricane Operations Plan (NHOP). The right ordinates represent the total number of observations used for verification.

a smaller RMSE below 500 hPa in the *Hydro* experiment, and this improvement is also evident in the 12-h and 24-h forecasts. For the V wind field (Figure 8b), the improvement, however, is not found at all levels, and only some improvements are observed above 850 hPa. This may be related to the large rejection of LWP observations, which mainly contribute to lower levels. For temperature (Figure 8c) and specific humidity (Figure 8d), the improvements are more pronounced and consistent in the *Hydro* experiment. Smaller RMSEs can be seen at the whole levels in both temperature and specific humidity analyses compared to the *CNTL* experiment. The RMSEs increase from analysis to 24-h forecast, but the RMSEs of the *Hydro* experiment are always smaller than those of the *CNTL* experiment.

The vertical profiles of RMSE of Hurricane Maria (2017) are shown in Figure 9. For the wind (Figures 9a and 9b), assimilating LWP and IWP has slight improvements on both the low-level wind analysis. As the forecast proceeds, the U wind field in the *Hydro* experiment can maintain some of the low-level advan-

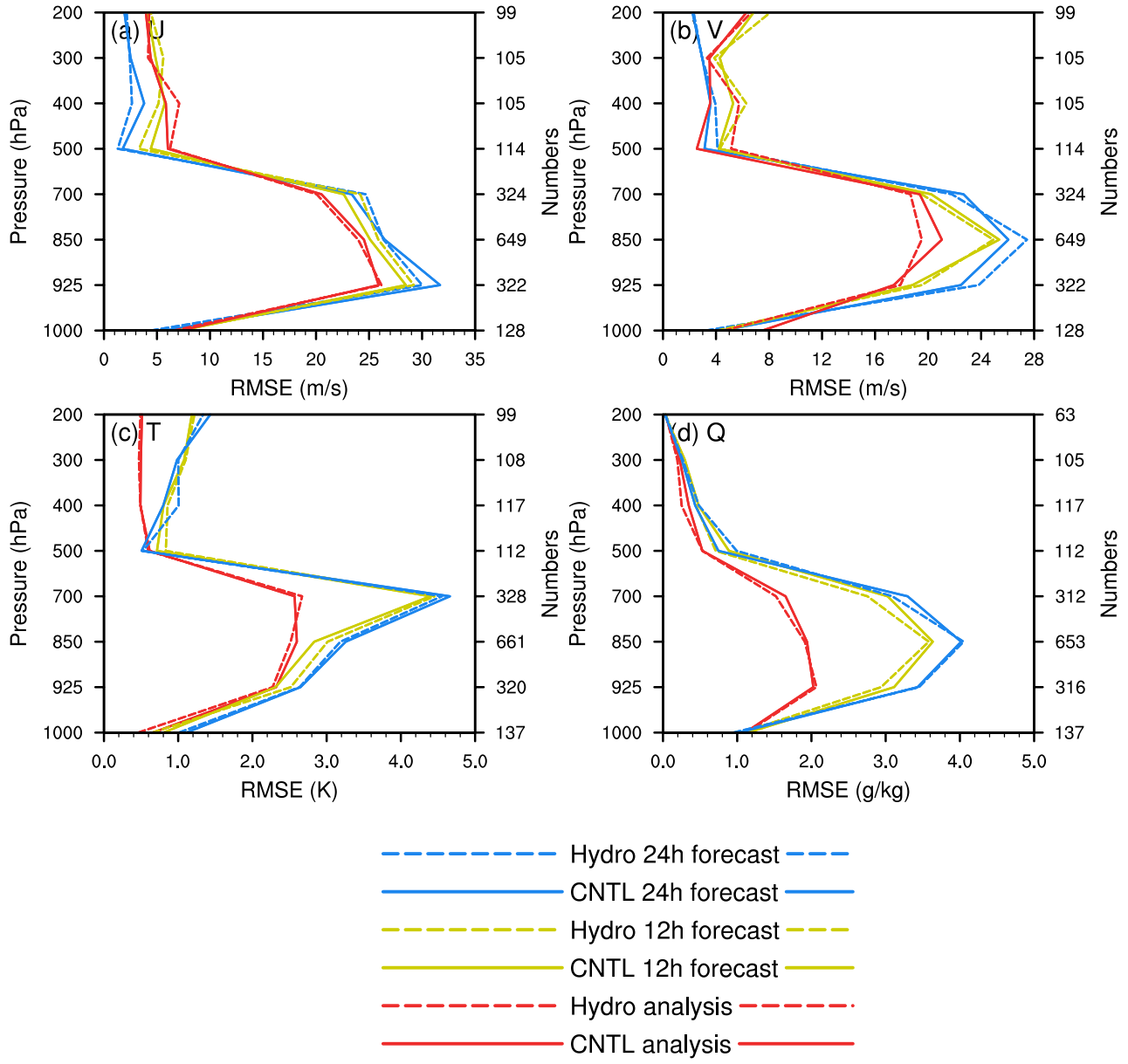

Figure 9. The same as Figure 8 but for Hurricane Maria (2017).

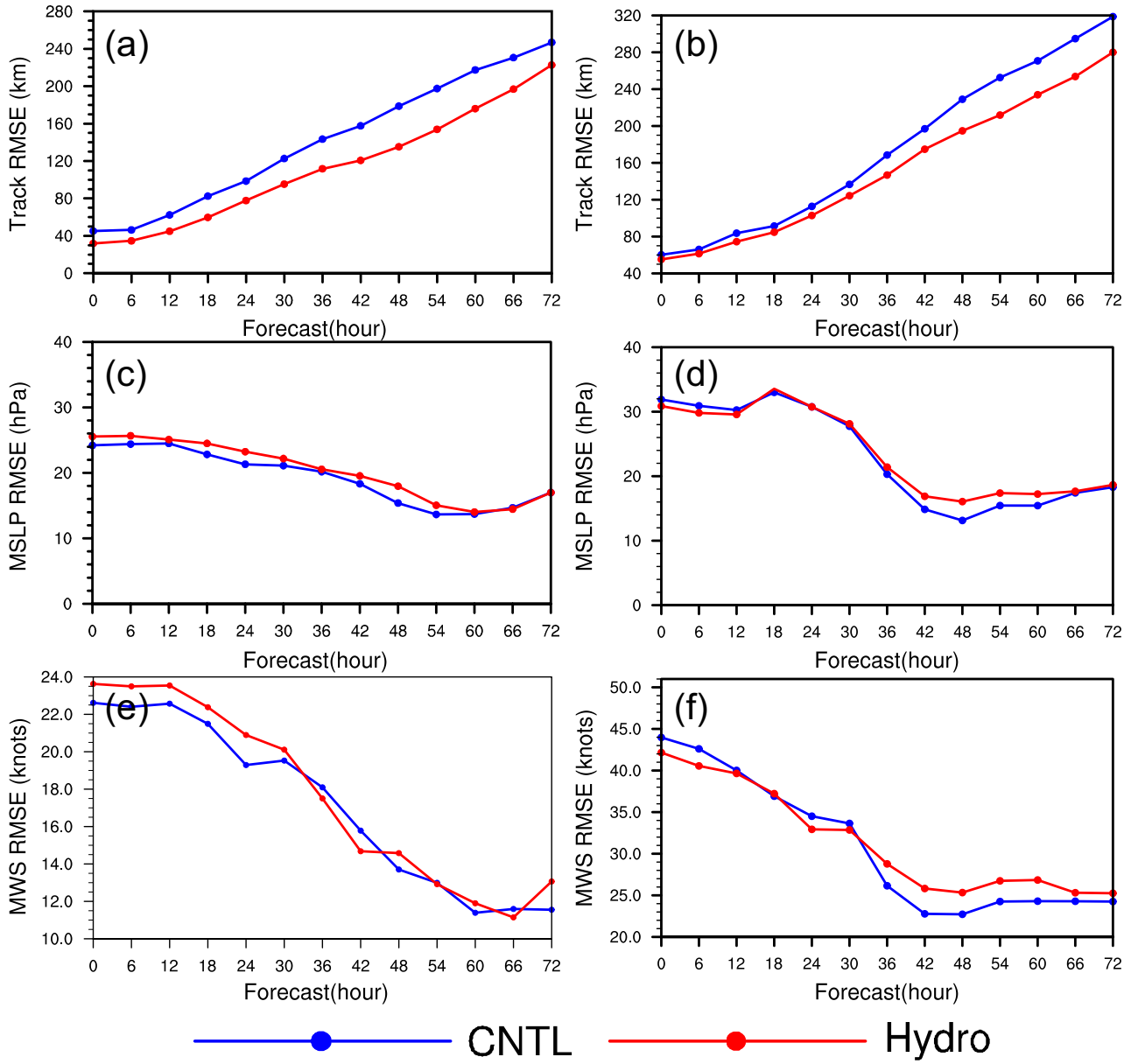

Figure 10. The (a), (b) track, (c), (d) minimum sea-level pressure (SLP), and (e), (f) 10 m maximum wind speed (MWS) forecast RMSE for the *CNTL* experiment (blue) and the *Hydro* experiment (red) for (a), (c), (e) Hurricane Irma (2017) and (b), (d), (f) Hurricane Maria (2017). The minimum (maximum) SLP (MWS) is found based on the Geophysical Fluid Dynamics Laboratory (GFDL) vortex standard method.

tages in the 24-h forecast, while the advantage of the V wind field in the Hydro experiment survives for a shorter time. For temperature (Figure 9c), slight improvements can be found in the analysis of the Hydro experiment below 850 hPa, but the errors of the two experiments tend to converge after the 24-h forecast. Compared to the *CNTL* experiment, the improvement of water vapor (Figure 9d) in the *Hydro* experiment is more obvious, and the error in the Hydro experiment is smaller than that in the *CNTL* experiment in both the analysis and forecast fields.

The verifications with the dropsonde observations illustrate that the assimilation of LWP and IWP with the new LWP and IWP operators not only improves the water vapor initialization but can also transfer the positive improvements to other forecast variables through model forecasts.

5.4. Impact on Hurricane Track and Intensity Forecasts

To assess the impact of the new LWP and IWP operators on the hurricane track and intensity forecasts, 72-h forecasts are made after each analysis step. The forecast RMSEs of hurricane track and intensity [characterized by minimum sea-level pressure (SLP) and the 10 m maximum wind speed (MWS)] are calculated compared to NHC best track dataset and shown in Figure 10. For the hurricane track, the tracking errors of the *Hydro* experiment are consistently smaller than that of the *CNTL* experiment both for Hurricane Irma (2017) and Hurricane Maria (2017). The RMSEs of track errors are reduced by about 20% on average.

For intensity errors, they decrease gradually with the forecast, which may be associated with the weakening of the two hurricanes. The model simulates hurricane weakening better compared to hurricane intensification, so the intensity error has a larger value at the initial time and gradually decreases as the forecast proceeds. Besides, the *Hydro* experiment gives comparable or slightly worse intensity results than the *CNTL* for both hurricanes. This should be related to the assimilated LWP and IWP data locations. Most of the assimilated LWP and IWP data are located around the hurricane, not in the inner core area as shown in Figure 6d, which helps to improve the environmental fields (Figures 8 and 9). The improved environments flow further leads to the hurricane track forecast improvement. However, missing the LWP and IWP data inside the storm benefit little to the intensity improvement for both strong hurricane cases.

To further quantify the impacts of the new LWP and IWP operators on hurricane forecasts, the improvement ratios are calculated for every 6-h forecast similar to the quantification method of Wang et al. (2019), but taking into account both MWS and SLP as intensity metrics

$$Improve\ Ratio = \left(\frac{RMSE\ of\ CNTL\ track\ -\ RMSE\ of\ Hydro\ track}{RMSE\ of\ CNTL\ track} \times \frac{1}{2} + \frac{RMSE\ of\ CNTL\ SLP\ -\ RMSE\ of\ Hydro\ SLP}{RMSE\ of\ CNTL\ SLP} \times \frac{1}{4} + \frac{RMSE\ of\ CNTL\ MWS\ -\ RMSE\ of\ Hydro\ MWS}{RMSE\ of\ CNTL\ MWS} \times \frac{1}{4} \right) \times 100\%$$

Figure 11 shows the improvement ratios for Hurricane Irma (2017) and Hurricane Maria (2017) for the 72 h forecast period. Overall, it is clear that the improvement ratios are positive for all forecast periods in Irma case and mostly positive in Maria case. Besides, the average improvement rates in Irma case for 6–24, 30–48, and 54–72 h gradually decreased, with the average values of 10.9%, 9.48%, and 7.35%, respectively. This indicates that the assimilation of LWP and IWP improves the Hurricane Irma (2017) forecast more effectively at the early stage. The decreasing improvement rates may be related to the self-adjustment of the model after assimilation of the hydrometeors information, where the LWP and IWP information gradually disappears with the forecast adjustment due to the lack of the necessary thermodynamic input support. Similar im-

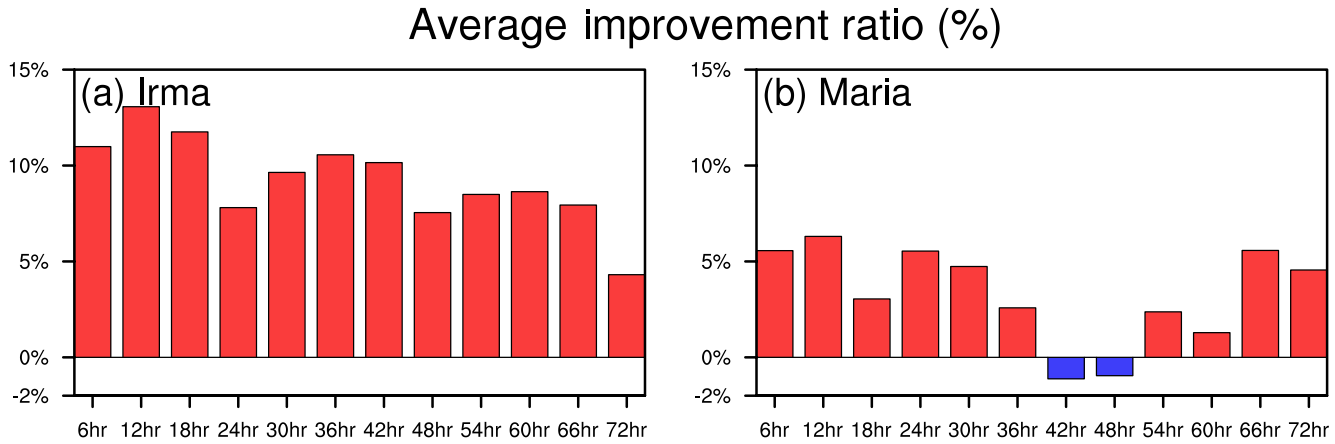

Figure 11. The improvement ratios for (a) Hurricane Irma (2017) and (b) Hurricane Maria (2017) at each forecast period.

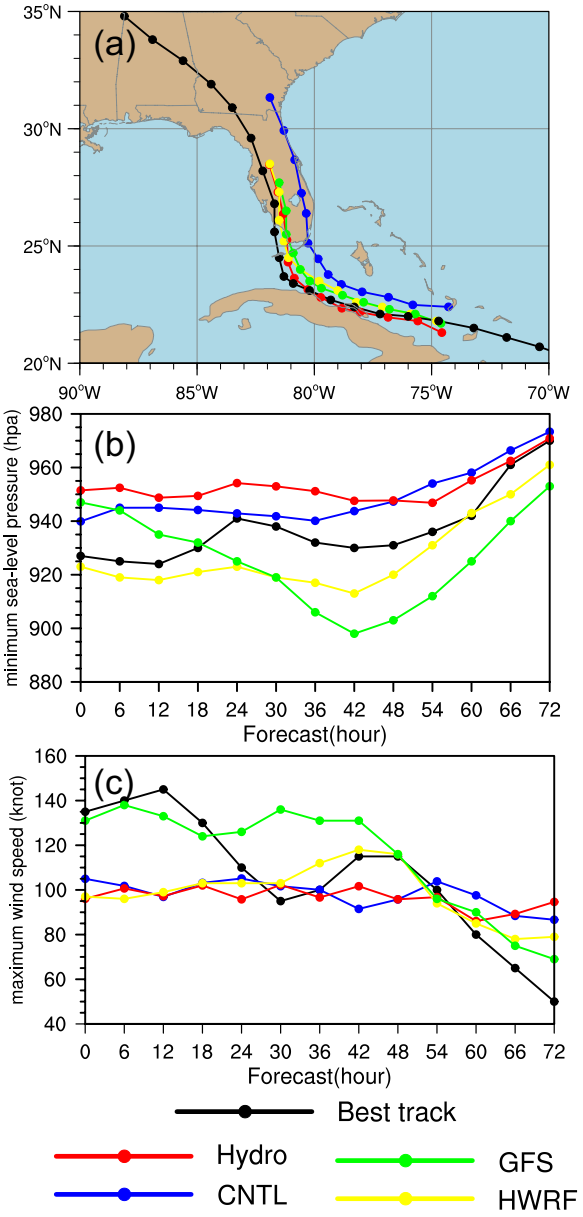

Figure 12. The Hurricane Irma (2017) forecast (a) tracks, (b) minimum sea-level pressure (hPa), and (c) maximum 10m wind speed (knot) of the *CNTL* experiment (blue), the *Hydro* experiment (red), GFS (green), and HWRF (yellow) start at 1200 UTC 08 September 2017 and the best track (black) is from the National Hurricane Center.

provement rate reduction can be found in the Maria case, with an average improvement rate of 5.11% in the 6–24 h and 3.45% in the 54–72 h. However, negative values of improvement rates are observed at 42 and 48 h, which are associated with a large intensity error at those periods.

In general, it shows that the assimilation of ABI-derived LWP and IWP using the new observation operator improves the forecast of Hurricanes, even if the intensity forecasts have slight negative contributions.

5.5. Impact Analysis on Hurricane Irma (2017)

To further explore the impact of assimilating ABI-derived LWP and IWP on hurricanes, we diagnose the analysis and forecast results of two experiments at 1200 UTC 08 September 2017, with the Irma case as an example.

Figure 12a shows the best track from the National Hurricane Center along with the 72-h track forecast from the *CNTL* experiment, the *Hydro* experiment, the Global Forecast System (GFS), and HWRF starting at 1200 UTC on 08 September 2017. Based on the best track, Hurricane Irma (2017) began by moving continuously northwest west (NWW), then turned north northwest (NNW), before making landfall in the southwest of the Florida Keys. However, the *CNTL* experiment predicts a consistent northern track compared to the best track, making landfall primarily in southeast Florida and striking eastern Florida. Both the GFS and HWRF predicted hurricane landfall on the west coast of Florida, but both had an early northeastward fold compared to the best track. After several cycles of assimilation, the initial position of Hurricane Irma (2017) in the *Hydro* experiment deviates less from the best track compared to the *CNTL* experiment. Subsequent track forecasts are highly fitting to the best track before the landfall, and landfall locations are also closer to observations.

The intensity forecasts vary widely in *CNTL*, *Hydro*, and operational forecasts. For SLP, two operational forecasts overestimated the strength of Irma, especially the GFS forecast with the smallest SLP of 900 hPa. The *CNTL* and *Hydro* experiments, on the other hand, insufficiently predict the intensity, especially the Hydro experiment, whose SLP prediction is weakest before 48 h. For MWS forecasts, the GFS performs best overall, while the HWRF predicts a weaker MWS up to 24 h compared to the best track. The CNTL and Hydro experiments are similar, with a weaker MWS forecast up to 54 h and a stronger one thereafter.

Since IWP dominates the strong convection, the high-level (300 hPa) water vapor analysis fields are compared between the *CNTL* and *Hydro* experiments (Figure 13). After several cycles of analysis, different structures of water vapor background fields have been obtained for the two experiments. Both intensity and range of the water vapor background at the hurricane core area in *Hydro* (Figure 13c) are smaller than those in *CNTL* (Figure 13a). The large water vapor ring band of *Hydro* is closer to the hurricane center than that of *CNTL*. After assimilation, there is no significant change in the range and intensity of water vapor in *CNTL* (Figure 13b) because of the sparse conventional observations over the sea. However, both the intensity and range of water vapor are considerably enhanced after the assimilation of LWP and IWP (Figure 13d). The enhancement of water vapor would further contribute to the prediction of the temperature and geopotential height fields through the latent heat release.

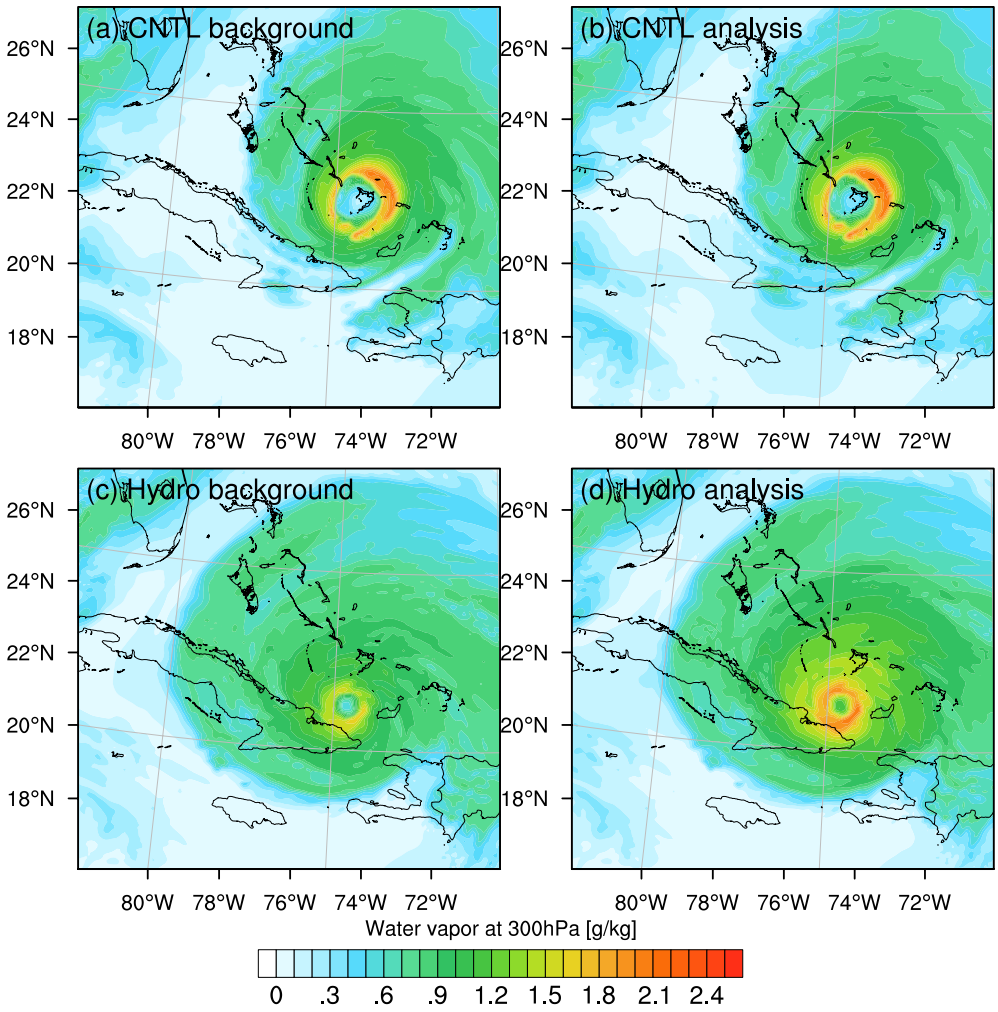

Figure 13. The water vapor (a), (c) background and (b), (d) analysis fields at 300 hPa of (a), (b) the *CNTL* experiment and (c), (d) the *Hydro* experiment at 1200 UTC 08 September 2017.

The temperature and geopotential heights at 500 hPa pressure level from the forecast beginning at 1200 UTC 08 September 2017 are plotted in Figure 14. After a 24 h forecast, the *CNTL* experiment (Figure 14a) shows a larger warm-core area, which is favorable for hurricane development. Thus, the hurricane in *CNTL* broke the northern geopotential heights early, while the geopotential height field remains continuous in the Hydro experiment (Figure 14b). The continuous geopotential heights field provides a barrier against the early northward movement of the hurricane. In the 48-h forecast field, the hurricane in the *CNTL* experiment (Figure 14c) has made early landfall and strikes southeastern Florida. Whereas the hurricane in the *Hydro* experiment (Figure 14d) still maintains a small distance from observations and is beginning to make landfall in southwest Florida. In the 72-h forecast, the warm core area becomes larger in *CNTL* (Figure 14e), while it is more concentrated in the center of the hurricane in *Hydro* (Figure 14f). Besides, the hurricane position maintains closer to the observation in the Hydro experiment than that in the *CNTL* experiment.

Based on the above analysis of the atmospheric fields, it can be seen that the ABI-derived cloud products are effectively assimilated through the new LWP and IWP observation operators. The water vapor field is first adjusted, and the changes in water vapor, in turn, affect the prediction of temperature and geopotential heights fields, leading to more accurate track forecasts.

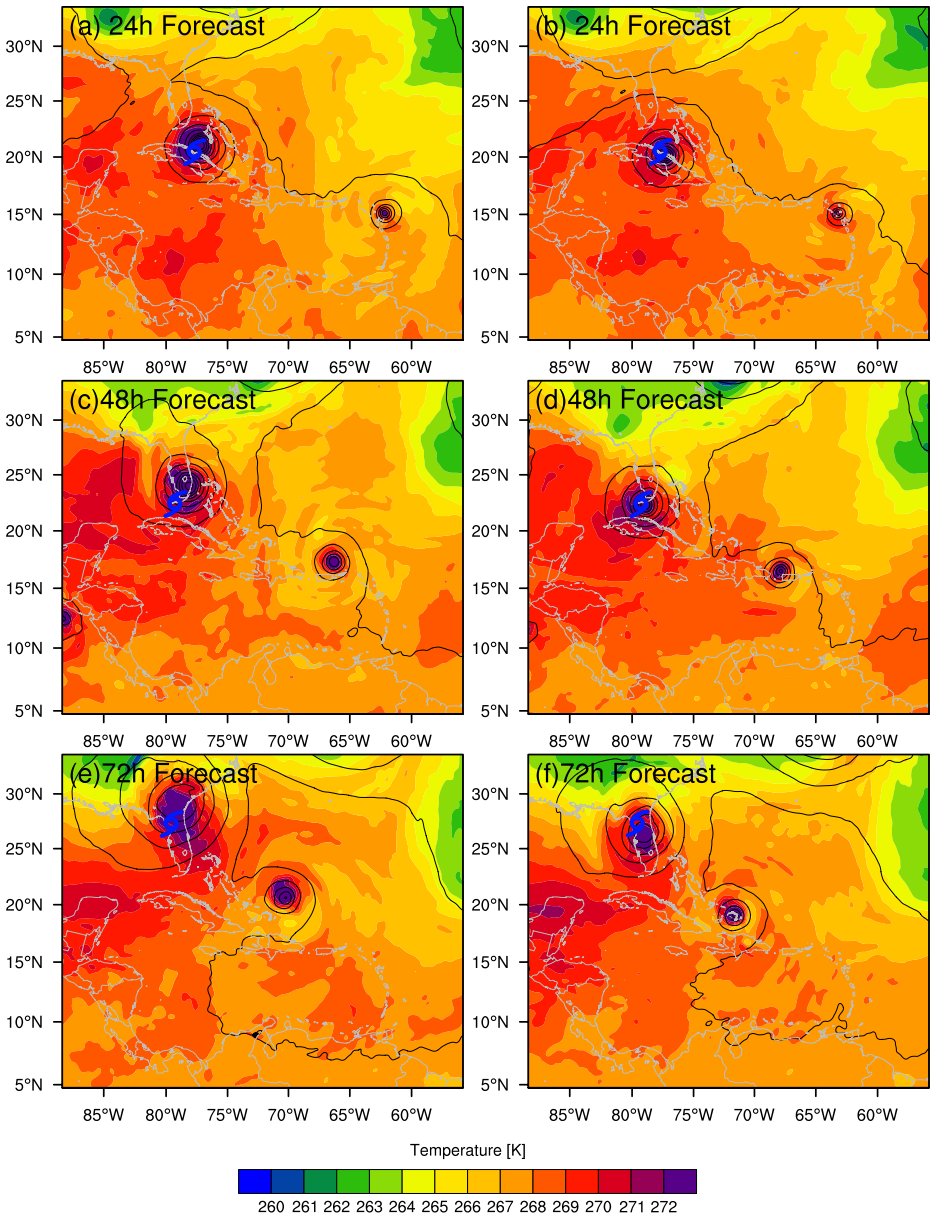

Figure 14. Temperature (shaded, unit: (k), geopotential height (contour, unit: m^2/s^2) at 500 hPa for (a), (b) 24h, (c), (d) 48h, and (e), (f) 72h forecasts from (a), (c), (e) the *CNTL* experiment and the *Hydro* experiment (b), (d), (f) start at 1200 UTC 08 September 2017. The hurricane center from best track is marked as blue at each time.

6. Summary

The LWP and IWP derived from the ABI onboard GOES-16 provide valuable observational information for hurricane initialization. However, how to effectively assimilate the LWP and IWP observations is an important new study topic.

In a previous study with GSI/HWRF, T. C. Wu et al. (2016) developed the SWC and LWC operators by using temperature, water vapor, and pressure and further derived the hydrometeors with an empirical formula. Their attempts successfully assimilated the cloud product observations but contained the negative hydrometeor simulation bias since the water vapor outputs from the model already exclude the hydrometeor information during the microphysical parameterization. To better describe the hydrometeors of the model, this study develops a pair of new LWP and IWP observation operators for the DTC-GSI data assimilation

system. The operators enable the use of the background hydrometeors information from the WRF-ARW model directly. Without adding extra control variables, the hydrometeors can be formulated from the water vapor by assuming the fixed hydrometeors proportions during the assimilation process. The simulated LWP and IWP can then be calculated by the vertical integration of cloud liquid/ice water content, respectively, while the moisture fields are modified by the assimilation of LWP and IWP data. Besides, the vertical propagation of analysis increment can be achieved by the Jacobian calculation of the LWP and IWP observation operators, which are confirmed by the Jacobian's analysis and a set of single observation experiments.

The impact studies of the cycling data assimilation and forecast experiments for Hurricane Irma (2017) and Hurricane Maria (2017) show that the new LWP and IWP observation operators can not only effectively enable the assimilation of ABI-derived LWP and IWP to reduce the bias between the simulated and observed LWP and IWP observations, but also improve the analysis and forecast accuracy by transferring cloud observations information to other model forecast variables in subsequent forecasts. In these two specific hurricane cases, the assimilation of LWP and IWP with new operators effectively improves hurricane forecasts overall by accounting for both path and intensity errors, with the improvements in track forecasts being more pronounced. The impact analysis shows that the assimilation of LWP and IWP improves the track prediction through influencing water vapor and thus influencing temperature and geopotential heights fields in subsequent forecasts.

This paper validates the new LWP and IWP operators based on Hurricane Irma (2017) and Hurricane Maria (2017). It is obvious that more convective cases should be included in future studies to generalize the validity of the new LWP and IWP operators. Finally, it needs to be pointed that while important, a more detailed understanding in the influence of the microphysics parameterization scheme on the new LWP and IWP operators is necessary but not the primary goal of this paper. To achieve such a goal, more comprehensive experiments and more detailed analyses on extreme weather events, such as severe local storms, are required.

Data Availability Statement

L1b data are from the SSEC data center (https://www.ssec.wisc.edu/datacenter/dcmain.html). The FNL data are obtained from NCEP (https://rda.ucar.edu/datasets/ds083.2/).

Acknowledgments
The GOES-16 LWP and IWP data were generated by the GOES-R AWG Cloud Team at the University of Wisconsin-Madison. The software to run the data is from NOAA/UW. This work was jointly sponsored by the National Key Research and Development Program of China (2017YFC1502102, 2018YFC1506803) (Y. Chen), SSEC Internal funding program, and NOAA GOES-R Risk Reduction (GOES-R3) (NA15NES4320001), China Scholarship Council (CSC) under the Grant No. N201808320281, and Postgraduate Research & Practice Innovation Program of Jiangsu Province (SJKY19_0936) (D. Meng). The view, opinions, and findings contained in this report are those of the authors and should not be construed as an official National Oceanic and Atmospheric Administration's or U.S. government's position, policy, or decision. Our deepest gratitude goes to the anonymous reviewers for their careful work and thoughtful suggestions that have helped improve this paper substantially. Besides, Tingchi Wu is also greatly appreciated for her helpful assistance in this study.

References

Bennartz, R. (2007). Global assessment of marine boundary layer cloud droplet number concentration from satellite. *Journal of Geophysical Research*, *112*. https://doi.org/10.1029/2006JD007547

Bernardet, L., Nance, L., Demirtas, M., Koch, S., Szoke, E., Fowler, T., et al. (2008). The Developmental Testbed Center and its winter forecasting experiment. *Bulletin of the American Meteorological Society*, *89*, 611–628. https://doi.org/10.1175/BAMS-89-5-611

Biswas, M. K., Bernardet, L., & Dudhia, J. (2014). Sensitivity of hurricane forecasts to cumulus parameterizations in the HWRF model. *Geophysical Research Letters*, *41*(24), 9113–9119. https://doi.org/10.1002/2014GL062071

Chen, Y., Wang, H., Min, J., Huang, X.-Y., Minnis, P., Zhang, R., et al. (2015). Variational assimilation of cloud liquid/ice water path and its impact on NWP. *Journal of Applied Meteorology and Climatology*, *54*, 1809–1825. https://doi.org/10.1175/jamc-d-14-0243.1

Chen, Y., Zhang, R., Meng, D., Min, J., & Zhang, L. (2016). Variational assimilation of satellite cloud water/ice path and microphysics scheme sensitivity to the assimilation of a rainfall case. *Advances in Atmospheric Sciences*, *33*, 1158–1170. https://doi.org/10.1007/s00376-016-6004-3

Desroziers, G., Berre, L., Chapnik, B., & Poli, P. (2005). Diagnosis of observation, background and analysis-error statistics in observation space. *Quarterly Journal of the Royal Meteorological Society*, *131*, 3385–3396. https://doi.org/10.1256/qj.05.108

Dudhia, J. (1989). Numerical study of convection observed during the winter monsoon experiment using a mesoscale two-dimensional model. *Journal of the Atmospheric Sciences*, *46*, 3077–3107. https://doi.org/10.1175/1520-0469(1989)046<3077:nsocod>2.0.co;2

Ebert, E. E., & Curry, J. A. (1992). A parameterization of ice cloud optical properties for climate models. *Journal of Geophysical Research*, *97*, 3831–3836. https://doi.org/10.1029/91JD02472

Errico, R. M., Bauer, P., & Mahfouf, J.-F. (2007). Issues regarding the assimilation of cloud and precipitation data. *Journal of the Atmospheric Sciences*, *64*, 3785–3798. https://doi.org/10.1175/2006jas2044.1

Gasperoni, N. A., Wang, X., & Wang, Y. (2020). A comparison of methods to sample model errors for convection-allowing ensemble forecasts in the setting of multiscale initial conditions produced by the GSI-Based EnVar assimilation system. *Monthly Weather Review*, *148*, 1177–1203. https://doi.org/10.1175/MWR-D-19-0124.1

Geer, A. J., Baordo, F., Bormann, N., Chambon, P., English, S. J., Kazumori, M., et al. (2017). The growing impact of satellite observations sensitive to humidity, cloud and precipitation. *Quarterly Journal of the Royal Meteorological Society*, *143*, 3189–3206. https://doi.org/10.1002/qj.3172

Goodman, S. J., Schmit, T. J., Daniels, J., & Redmon, R. J. (2020). GOES-R series summary and look ahead. In *The GOES-R series* (pp. 273–277). Elsevier. https://doi.org/10.1016/b978-0-12-814327-8.00023-8

Hong, S.-Y., & Lim, J.-O. J. (2006). The WRF single-moment 6-class microphysics scheme (WSM6). *Journal of the Korean Meteorological Society*, *42*, 129–151

Hong, S.-Y., Noh, Y., & Dudhia, J. (2006). A new vertical diffusion package with an explicit treatment of entrainment processes. *Monthly Weather Review*, *134*, 2318–2341. https://doi.org/10.1175/mwr3199.1

Jones, T. A., & Stensrud, D. J. (2015). Assimilating cloud water path as a function of model cloud microphysics in an idealized simulation. *Monthly Weather Review*, *143*, 2052–2081. https://doi.org/10.1175/MWR-D-14-00266.1

Jones, T. A., Stensrud, D. J., Minnis, P., & Palikonda, R. (2013). Evaluation of a forward operator to assimilate cloud water path into WRF-DART. *Monthly Weather Review*, *141*, 2272–2289. https://doi.org/10.1175/MWR-D-12-00238.1

Kleist, D. T., Parrish, D. F., Derber, J. C., Treadon, R., Wu, W.-S., & Lord, S. (2009). Introduction of the GSI into the ncep global data assimilation system. *Weather and Forecasting*, *24*(6), 1691–1705. https://doi.org/10.1175/2009WAF2222201.1

Kostka, P. M., Weissmann, M., Buras, R., Mayer, B., & Stiller, O. (2014). Observation operator for visible and near-infrared satellite reflectances. *Journal of Atmospheric and Oceanic Technology*, *31*, 1216–1233. https://doi.org/10.1175/JTECH-D-13-00116.1

Kurzrock, F., Cros, S., Ming, F. C., Otkin, J. A., Hutt, A., Linguet, L., et al. (2018). A review of the use of geostationary satellite observations in regional-scale models for short-term cloud forecasting. *Meteorologische Zeitschrift*, *27*, 277–298. https://doi.org/10.1127/metz/2018/0904

Landsea, C. W., & Franklin, J. L. (2013). Atlantic hurricane database uncertainty and presentation of a new database format. *Monthly Weather Review*, *141*, 3576–3592. https://doi.org/10.1175/MWR-D-12-00254.1

Lee, J. R., Li, J., Li, Z., Wang, P., & Li, J. (2019). ABI water vapor radiance assimilation in a regional NWP model by accounting for the surface impact. *Earth and Space Science*, *6*(9), 1652–1666. https://doi.org/10.1029/2019EA000711

Li, J., Li, J., Velden, C., Wang, P., Schmit, T. J., & Sippel, J. (2020). Impact of rapid-scan-based dynamical information from GOES-16 on HWRF hurricane forecasts. *Journal of Geophysical Research - D: Atmospheres*, *125*(3). https://doi.org/10.1029/2019JD031647

Li, J., Li, Z., Wang, P., Schmit, T. J., Bai, W., & Atlas, R. (2017). An efficient radiative transfer model for hyperspectral IR radiance simulation and applications under cloudy-sky conditions. *Journal of Geophysical Research - D: Atmospheres*, *122*, 7600–7613. https://doi.org/10.1002/2016JD026273

Li, J., Liu, C. Y., Huang, H.-L., Schmit, T. J., Menzel, W. P., & Gurka, J. (2005). Optimal cloud-clearing for AIRS radiances using MODIS. *IEEE Transactions On Geoscience and Remote Sensing*, *43*, 1266–1278.

Li, J., Wang, P., Han, H., Li, J., & Zheng, J. (2016). On the assimilation of satellite sounder data in cloudy skies in numerical weather prediction models. *Journal of Meteorological Research*, *30*, 169–182. https://doi.org/10.1007/s13351-016-5114-2

Lin, B., & Rossow, W. B. (1996). Seasonal variation of liquid and ice water path in nonprecipitating clouds over oceans. *Journal of Climate*, *9*, 2890–2902. https://doi.org/10.1175/1520-0442(1996)009<2890:SVOLAI>2.0.CO;2

Meng, D., Chen, Y., Wang, H., Gao, Y., Potthast, R., & Wang, Y. (2019). The evaluation of EnVar method including hydrometeors analysis variables for assimilating cloud liquid/ice water path on prediction of rainfall events. *Atmospheric Research*, *219*, 1–12. https://doi.org/10.1016/j.atmosres.2018.12.017

Michael, P. (2010). *GOES-R advanced baseline imager (ABI) algorithm theoretical basis document for cloud type and cloud phase*. Retrieved from https://www.star.nesdis.noaa.gov/goesr/documents/ATBDs/Baseline/ATBD_GOES-R_Cloud_Phase_Type_v2.0_Sep2010.pdf

Migliorini, S. (2012). On the equivalence between radiance and retrieval assimilation. *Monthly Weather Review*, *140*, 258–265. https://doi.org/10.1175/MWR-D-10-05047.1

Minamide, M., & Zhang, F. (2017). Adaptive observation error inflation for assimilating all-sky satellite radiance. *Monthly Weather Review*, *145*(3), 1063–1081. https://doi.org/10.1175/MWR-D-16-0257.1

Minamide, M., & Zhang, F. (2019). An adaptive background error inflation method for assimilating all-sky radiances. *Quarterly Journal of the Royal Meteorological Society*, *145*(719), 805–823. https://doi.org/10.1002/qj.3466

Minnis, P. (2007). Cloud retrievals From GOES-R. In *Fourier Transform Spectroscopy/Hyperspectral imaging and sounding of the environment*. Santa Fe, New Mexico: OSA. https://doi.org/10.1364/hise.2007.hwc3

Minnis, P., Nguyen, L., Palikonda, R., Heck, P. W., Spangenberg, D. A., Doelling, D. R., et al. (2008). Near-real time cloud retrievals from operational and research meteorological satellites. In R. H. Picard, A. Comeron, K. Schäfer, A. Amodeo, & M. van Weele, (Eds.), *Presented at the SPIE Remote Sensing, Cardiff, Wales, United Kingdom* (p. 710703). https://doi.org/10.1117/12.800344

Minnis, P., Sun-Mack, S., Young, D. F., Heck, P. W., Garber, D. P., Chen, Y., et al. (2011). CERES Edition-2 cloud property retrievals using TRMM VIRS and Terra and Aqua MODIS Data-Part I: Algorithms. *IEEE Transactions on Geoscience Remote Sensing*, *49*, 4374–4400. https://doi.org/10.1109/TGRS.2011.2144601

Mlawer, E. J., Taubman, S. J., Brown, P. D., Iacono, M. J., & Clough, S. A. (1997). Radiative transfer for inhomogeneous atmospheres: RRTM, a validated correlated-k model for the longwave. *Journal of Geophysical Research*, *102*, 16663–16682. https://doi.org/10.1029/97jd00237

OFCM. (2017). Retrieved from https://www.icams-portal.gov/publications/nhop/FCM-P12-2017.pdf

Otkin, J. A. (2010). Clear and cloudy sky infrared brightness temperature assimilation using an ensemble Kalman filter. *Journal of Geophysical Research*, *115*(D19). https://doi.org/10.1029/2009JD013759

Otkin, J. A. (2012). Assimilation of water vapor sensitive infrared brightness temperature observations during a high impact weather event. *Journal of Geophysical Research*, *117*(D19), n/a–n/a. https://doi.org/10.1029/2012JD017568

Rappaport, E. N., Franklin, J. L., Avila, L. A., Baig, S. R., Beven, J. L., Blake, E. S., et al. (2009). Advances and challenges at the National Hurricane Center. *Weather and Forecasting*, *24*, 395–419. https://doi.org/10.1175/2008WAF2222128.1

Sanabia, E. R., Barrett, B. S., Black, P. G., Chen, S., & Cummings, J. A. (2013). Real-time upper-ocean temperature observations from aircraft during operational hurricane reconnaissance missions: AXBT demonstration project year one results. *Weather and Forecasting*, *28*, 1404–1422. https://doi.org/10.1175/WAF-D-12-00107.1

Schmit, T. J., Griffith, P., Gunshor, M. M., Daniels, J. M., Goodman, S. J., & Lebair, W. J. (2017). A closer look at the ABI on the GOES-R series. *Bulletin of the American Meteorological Society*, *98*(4), 681–698. https://doi.org/10.1175/BAMS-D-15-00230.1

Schmit, T. J., Gunshor, M. M., Menzel, W. P., Gurka, J. J., Li, J., & Bachmeier, A. S. (2005). Introducing the next-generation advanced baseline imager on Goes-r. *Bulletin of the American Meteorological Society*, *86*, 1079–1096. https://doi.org/10.1175/bams-86-8-1079

Tong, M., Sippel, J. A., Tallapragada, V., Liu, E., Kieu, C., Kwon, I.-H., et al. (2018). Impact of assimilating aircraft reconnaissance observations on tropical cyclone initialization and prediction using operational HWRF and GSI ensemble-variational hybrid data assimilation. *Monthly Weather Review*, *146*, 4155–4177. https://doi.org/10.1175/mwr-d-17-0380.1

Vonich, P. T., & Hakim, G. J. (2018). Hurricane kinetic energy spectra from in situ aircraft observations. *Journal of the Atmospheric Sciences*, *75*, 2523–2532. https://doi.org/10.1175/JAS-D-17-0270.1

Walther, A., & Heidinger, A. K. (2012). Implementation of the daytime cloud optical and microphysical properties algorithm (DCOMP) in PATMOS-x. *The Journal of Applied Meteorology and Climatology*, *51*, 1371–1390. https://doi.org/10.1175/JAMC-D-11-0108.1

Walther, A., Heidinger, A. K., & Miller, S. (2013). The expected performance of cloud optical and microphysical properties derived from Suomi NPP VIIRS day/night band lunar reflectance. *Journal of Geophysical Research - D: Atmospheres*, *118*, 230–313. https://doi.org/10.1002/2013JD020478

Walther, A., Straka, W., & Heidinger, A. K. (2013). *ABI algorithm theoretical basis document for daytime cloud optical and microphysical properties (DCOMP)*. Retrieved from https://www.star.nesdis.noaa.gov/goesr/documents/ATBDs/Baseline/ATBD_GOES-R_Cloud_DCOMP_v3.0_Jun2013.pdf

Wang, P., Li, J., Goldberg, M. D., Schmit, T. J., Lim, A. H. N., Li, Z., et al. (2015). Assimilation of thermodynamic information from advanced infrared sounders under partially cloudy skies for regional NWP. *Journal of Geophysical Research - D: Atmospheres*, *120*, 5469–5484. https://doi.org/10.1002/2014JD022976

Wang, P., Li, J., Li, Z., Lim, A. H. N., Li, J., & Goldberg, M. D. (2019). Impacts of observation errors on hurricane forecasts when assimilating hyperspectral infrared sounder radiances in partially cloudy skies. *Journal of Geophysical Research - D: Atmospheres*, *124*, 10802–10813. https://doi.org/10.1029/2019JD031029

Wang, P., Li, J., Li, Z., Lim, A. H. N., Li, J., Schmit, T. J., & Goldberg, M. D. (2017). The impact of cross-track infrared sounder (CrIS) cloud-cleared radiances on hurricane Joaquin (2015) and Matthew (2016) forecasts. *Journal of Geophysical Research - D: Atmospheres*, *122*, 201–213. https://doi.org/10.1002/2017JD027515

Wang, Z., & Sassen, K. (2002). Cirrus cloud microphysical property retrieval using lidar and radar measurements. Part I: Algorithm description and comparison with in situ data. *Journal of Applied Meteorology*, *41*, 12. https://doi.org/10.1175/1520-0450(2002)041<0218:CCMPRU>2.0.CO;2

Wu, T.-C., & Zupanski, M. (2017). Assimilating GPM hydrometeor retrievals in HWRF: choice of observation operators. *Atmospheric Science Letters*, *18*, 238–245. https://doi.org/10.1002/asl.748

Wu, T.-C., Zupanski, M., Grasso, L. D., Brown, P. J., Kummerow, C. D., & Knaff, J. A. (2016). The GSI capability to assimilate TRMM and GPM hydrometeor retrievals in HWRF. *Quarterly Journal of the Royal Meteorological Society*, *142*, 2768–2787. https://doi.org/10.1002/qj.2867

Wu, T.-C., Zupanski, M., Grasso, L. D., Kummerow, C. D., & Boukabara, S.-A. (2019). All-sky radiance assimilation of ATMS in HWRF: A demonstration study. *Monthly Weather Review*, *147*, 85–106. https://doi.org/10.1175/MWR-D-17-0337.1

Wu, W.-S., Purser, R. J., & Parrish, D. F. (2002). Three-dimensional variational analysis with spatially inhomogeneous covariances. *Monthly Weather Review*, *130*, 2905–2916. https://doi.org/10.1175/1520-0493(2002)130<2905:TDVAWS>2.0.CO;2

Yang, C., Liu, Z., Gao, F., Childs, P. P., & Min, J. (2017). Impact of assimilating GOES imager clear-sky radiance with a rapid refresh assimilation system for convection-permitting forecast over Mexico. *Journal of Geophysical Research - D: Atmospheres*, *122*(10), 5472–5490. https://doi.org/10.1002/2016JD026436

Yucel, I., James Shuttleworth, W., Gao, X., & Sorooshian, S. (2003). Short-term performance of MM5 with cloud-cover assimilation from satellite observations. *Monthly Weather Review*, *131*, 1797–1810. https://doi.org/10.1175//2565.1

Yucel, I., Shuttleworth, W. J., Pinker, R. T., Lu, L., & Sorooshian, S. (2002). Impact of ingesting satellite-derived cloud cover into the regional atmospheric modeling system. *Monthly Weather Review*, *130*, 19. https://doi.org/10.1175/1520-0493(2002)130<0610:IOISDC>2.0.CO;2

Zhu, Y., Liu, E., Mahajan, R., Thomas, C., Groff, D., Van Delst, P., et al. (2016). All-sky microwave radiance assimilation in NCEP's GSI analysis system. *Monthly Weather Review*, *144*(12), 4709–4735. https://doi.org/10.1175/MWR-D-15-0445.1